The Thesis Committee for Cagdas Arlanoglu
Certifies that this is the approved version of the following thesis:

Casing Drilling and Modeling of Smear Effect

APPROVED BY
SUPERVISING COMMITTEE:

Supervisor: _____
Kenneth E. Gray

Co-Supervisor: _____
Evgeny Podnos

Casing Drilling and Modeling of Smear Effect

by

Cagdas Arlanoglu, B.S.

Thesis

Presented to the Faculty of the Graduate School of

The University of Texas at Austin

in Partial Fulfillment

of the Requirements

for the Degree of

Master of Science in Engineering

The University of Texas at Austin

December 2011

Dedication

To my family and friends

Acknowledgements

First and foremost, I would like to express my utmost thanks to my supervisor, Dr. Kenneth E. Gray for his support and supervision during my two years of master's study. I am very grateful for the opportunity to be part of this project and its experience and guidance.

I am also heartily grateful to Dr. Evgeny Podnos for his guidance, support and patience during this work. I want to thank him for his encouragement and prompt answers to my questions.

I also would like thank Dr. Eric Becker for his deep knowledge, kind help and valuable efforts in this project.

I am also grateful to my office colleagues; Berkay Kocababuc and Xiaoyan Shi for their friendship and supports during my two year study.

I also would like to express my thanks to Turkish Petroleum Corporation for providing me a full scholarship and financial support.

Finally, I would like to thank my family. This study would not be accomplished without their continued love and support throughout my life. I also would like to express my thanks to Cansu Iste for her endless love.

Abstract

Casing Drilling and Modeling of Smear Effect

Cagdas Arlanoglu, M.S.E

The University of Texas at Austin, 2011

Supervisor: Kenneth E. Gray

Co-Supervisor: Evgeny Podnos

Lost circulation and wellbore failure are common problems in the petroleum industry and they increase drilling costs dramatically. Casing drilling in depleted zones helps reduce drilling costs and problems related to lost circulation and wellbore failure. Thus, casing drilling is an important technology to minimize or eliminate conventional drilling problems in depleted zones.

This thesis is focused on a study of smear effect in casing drilling in depleted formations. It is based on information about casing drilling and a commercial computer software ABAQUS. The smearing mechanism of drilling solids into the wellbore wall and the effects of parameters that affect the stress distribution around the wellbore wall are studied.

Moreover, multiple wellbore cracks are studied to determine their effects on hoop stress distribution and all the results are given at the results chapter of this study. All the discussions about the changing parameters are given in results section.

In conclusion, the smear effect in casing drilling can significantly improve hoop stresses around the wellbore and lost circulation problems can be minimized by using casing as a drilling string. These models can be used as a basic tool to understand smear effects in casing drilling in depleted formations.

Table of Contents

List of Tables

List of Figures

1. Introduction

1.1. Overview Of Lost Circulation

Much of the world's known reserves of oil and natural gas are hard to drill economically and safely, even with today's technology and conventional tools. Also, the increasing number of depleted reservoirs around the world and increasing demand for energy encourage the oil and gas industry to continuously find new techniques to improve drilling technology. Ultra-deep environments often have lost circulation problems.

Lost circulation is the loss of a significant amount of drilling fluid commonly known as mud, into formations being drilled. Lost circulation is a common problem and costs millions of dollars annually to operators. According to Ivan et al. (2003), petroleum companies spend $800 million per year to combat lost circulation, and nearly $200 million of the cost is lost circulation products. Moreover, Rahman (2010) stated that, considerable amount of money has been spent to prevent and manage lost circulation and its bad consequences such as rig time loss, kicks, blow-outs, and killing valuable wells. Lost circulation increases non-productive time for conventional drilling especially in offshore drilling for which rig costs are much higher. Wang (2007) states that lost circulation in Gulf of Mexico shelf drilling is 12 % of non-productive time and even more.

In general, lost circulation occurs when the pressure of the hydrostatic column is higher than formation pore pressure. Also, lost circulation occurs when the equivalent circulation density (ECD) overcomes the fracture gradient. In depleted formations, the pressure difference between the fracture pressure and the pore pressure is small and these formations are much more sensitive to lost circulation problems.

1.1.1. Lost Circulation Types

In general, drilling companies classify the lost circulations into four categories.

- Seepage losses
- Filtrate losses
- Vugular losses
- Fracture propagation losses

In seepage losses drilling fluid leaks into the pore spaces; as shown in Figure 1. Those kinds of losses are generally seen in highly permeable and depleted formations.

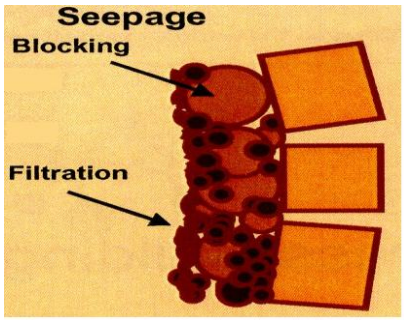

Figure 1. Seepage Losses (Zeilinger, 2010)

In filtrate losses, drilling fluid also leaks into the pore throats but if the mud particles sizes are too large to penetrate into the formation, there is only seepage of filtrate from the drilling fluid.

Another type of lost circulation is vugular losses. In vugular losses, a great amount of drilling fluid flows into the large openings. These kinds of losses are often seen in limestone formations that are broken and dissolved over geologic time. Vugular losses are illustrated in Figure 2.

Figure 2 Vugular losses (Zeilinger, 2010)

The last and most important lost circulation type is fracture propagation losses. A fracture is generated when the wellbore pressure exceeds the tensile strength of a rock. If a fracture is generated, increasing mud pressure in a well can cause fracture propagation. The fracture pressure of the formation and the pore pressure difference is small in a depleted formation, and fractures are often generated while drilling through depleted zones. Significant losses generally happen through fracture propagation. According to Dupriest (2005), notwithstanding the other types of losses (vugular, matrix seepage, and filtrate loss) over 90% of lost return expenses are related to fracture propagation. Figure 3 demonstrates the four types of lost circulations.

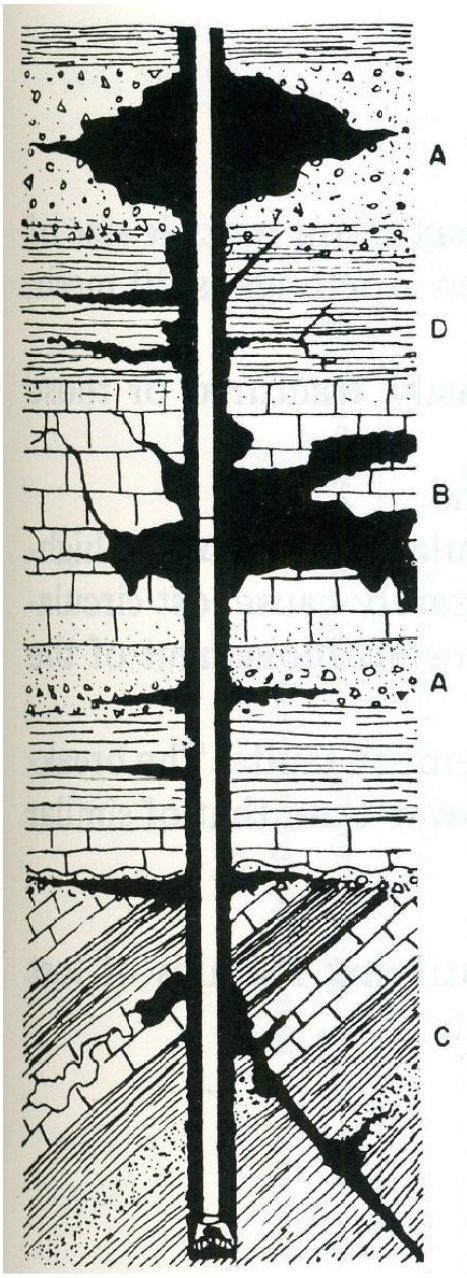

Figure 3 Types of lost circulations: A. very permeable unconsolidated formations, B. vugular formations, C. faulted, jointed formations, D. induced fractured formations (Chilingarian et al., 1983)

1.1.2. Effects of Lost Circulation

Lost circulation has several considerable consequences. When lost circulation happens, the hydrostatic pressure of the drilling fluid column is reduced. Because hydrostatic head pressure is reduced, formations fluids may flow into the well. When fluid flowing into the well cannot be controlled, blow-outs are expected at the surface and sometimes the well is lost. Moreover, lost circulation causes differential sticking because of collapsing the well. When drilling fluid pressure is low, the well may collapse and drilling tools may become stuck. Stuck pipes are often consequences of lost circulation, results in non-productive time (NPT) in the drilling operation.

1.2. WELLBORE STABILITY AND STRENGTHENING

Wellbore stability technology seeks to avoid plastic deformation and failure of the rock around a wellbore. The failure and plastic deformation result from mechanical stress altering and chemical reactions around the rock. During drilling or after drilling operations, the stresses in the rock around the wellbore change and stresses may become unstable. As a result, rock deforms as tensile or shear fractures are generated or the rock may be chemically altered by mud filtrate. According to the Amoco Wellbore Stability Drilling Handbook, companies spend between 600 million to 1 billion dollars annually because of hole stability problems. Figure 4 shows the classification of wellbore stability problems.

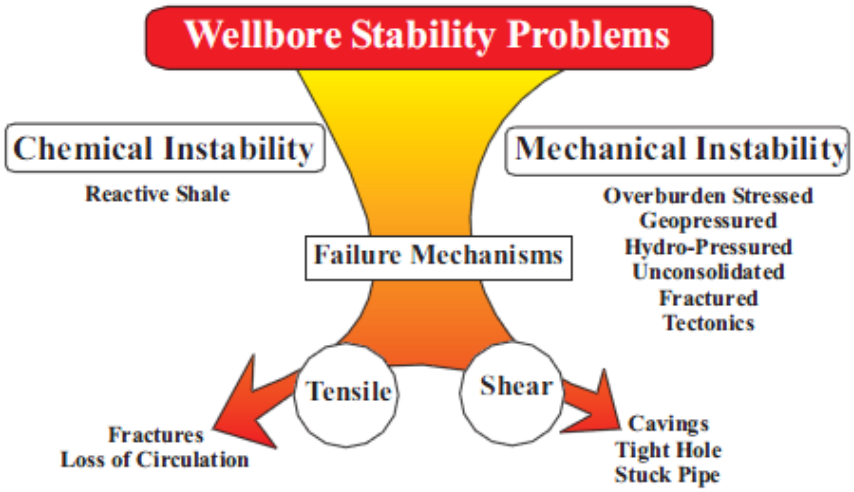

Figure 4. Wellbore stability problems classification (Amoco Wellbore Stability Drilling Handbook)

During the last decade, numerous techniques have been developed to reduce lost circulation and strengthen the wellbores. Wellbore strengthening means that the formation breakdown pressure or fracture gradient are increased by some operator actions. Several approaches can be used wellbore for strengthening treatments such as special granular materials; heating the wellbore; place pills; use mud that includes special bridging materials; and casing drilling. Aston et al. stated that (2007) "Emphasis on "wellbore strengthening" has been growing over the past few years, as reflected by the increase in frequency and variety of technologies that have been applied to this goal."

Also, drilling in depleted zones causes many problems. Sometimes it is impossible to drill in depleted zones because the mud weight needed to hold the pore pressure in neighboring zones causes an overbalanced situation, result in lost circulation. The goal is to increase the fracture gradient and prevent the lost of whole drilling fluids and other wellbore instabilities.

On the other hand, Wang et al. (2007) declared that the idea of wellbore strengthening helps operators indentify lost circulation and its treatment in a more useful way. Thus, operators can drill wells in loss known areas without an extra casing string, if wellbore strengthening can be consistently accomplished.

1.3. Purpose of This Study

One of the newest and useful technologies to prevent lost circulation and strengthen the wellbore is casing drilling. Moellendick and Karimi (2011) stated that casing drilling has been shown to eliminate or extremely minimize lost circulation and improve wellbore strength. The smear/ plastering effect concept is used to demonstrate the improvement in wellbore stability and eliminating lost circulation.

In this thesis, the smear/plastering effect in casing drilling in depleted formations is investigated. A finite element model in ABAQUS is used to understand the different aspects of plastering effects in casing drilling. By observing the stresses around wellbore, basic concepts of casing drilling are developed.

1.4. Outline of the Thesis

In introductory Chapter 1, information about lost circulation, types and effects are discussed. Also, wellbore stability and strengthening are seen included.

Chapter 2 gives information about casing drilling and the advantages and processes. Also, the plastering/smear effect in casing drilling in depleted formations is discussed.

Chapter 3 describes a physical model generated in ABAQUS with assumptions, boundary conditions and analysis.

Chapter 4 presents and discusses the ABAQUS model results.

Chapter 5 presents conclusions and recommendations for future works.

2. Casing Drilling

2.1. Overview of Casing Drilling

Casing drilling is a beneficial technology using the casing string as a drilling string. The well is drilled and cased simultaneously in casing while drilling operations. The casing string is rotated at the surface with a top drive and drilling fluid is circulated the same as in conventional drilling. This technology is generally used in depleted reservoirs that often have wellbore instability and lost circulation problems. Drilling with casing eliminates tripping and also lessens situations as kicks, differential sticking, and lost circulations could take place while tripping. According to Robinson et al. (2008) casing drilling is used successfully rather than conventional drilling method in the wells that were classified as undrillable with the conventional drilling techniques. Limbert et al. (2009) stated that over 200 wells have been drilled with casing drilling rigs and it was concluded that casing drilling reduced the lost circulation and non-productive time in depleted zones. In 2006 and 2007 casing drilling technology helped operators gain savings in drilling cost by 15 % while increasing the footage by 23 % per day. Figure 5 illustrates the casing drilling application.

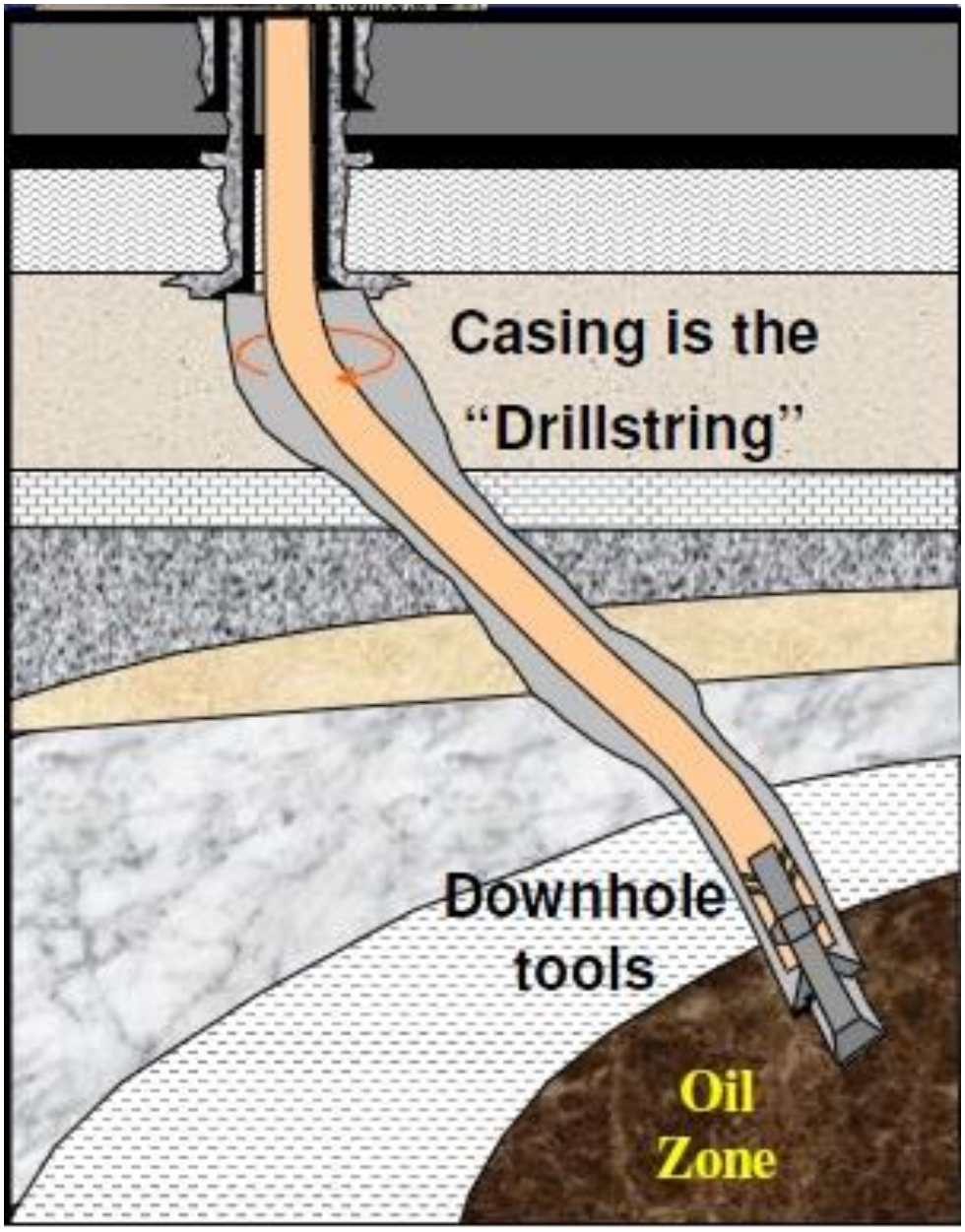

Figure 5. Casing drilling application (SPE Distinguished Lecturer Series)

2.2. CASING DRILLING PROCESS

In casing drilling process, the well is drilled with a casing string and cased simultaneously. The casing string is used as the drill string and a top drive mechanism provides the mechanical and hydraulic energy to the casing string and its pilot bit. Drilling fluid is circulated down through the casing string and circulated up through the annulus, which has a smaller annulus compared to conventional drilling. A casing drilling bottom hole assembly (BHA consists of a pilot bit, underreamer, and drill lock assembly (DLA). Figure 6 shows typical casing drilling BHA in a vertical well.

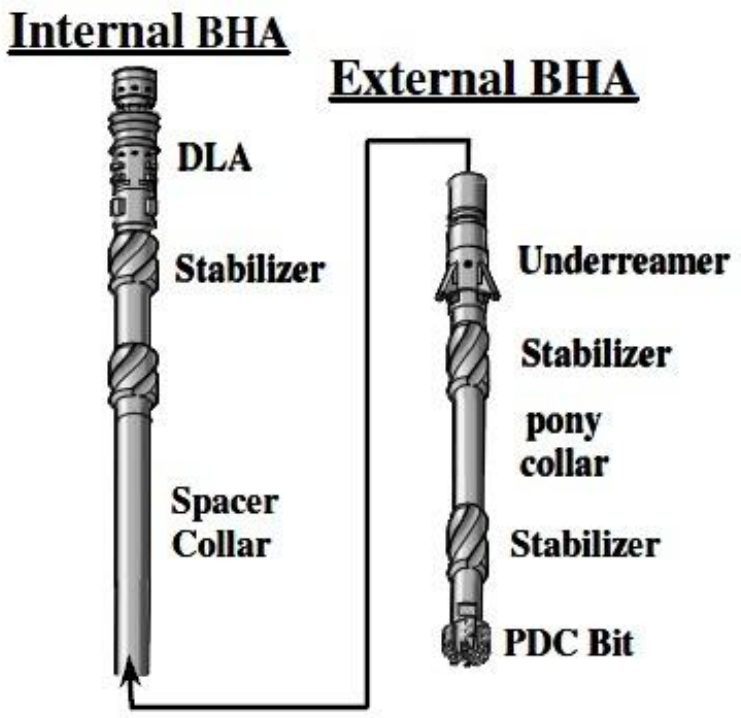

Figure 6. Casing drilling bottom hole assembly (BHA), (Warren and Lesso, 2005)

The drilling assembly and casing string are connected by a Drill Lock Assembly (DLA) which connects the casing with the BHA and seals the connections hydraulically. Figure 7 shows a DLA tool.

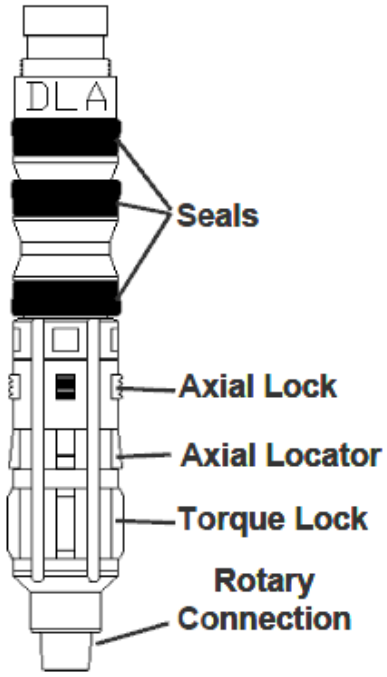

Figure 7. Drill-lock-assembly (DLA), (Warren et al., 2003)

There are two basic types of casing drilling systems;

- Retrievable System
- Non-retrievable System

In a retrievable system, the bottom hole assembly (BHA), the first joint of the casing string is connected to the BHA with a DLA. At total depth the bottom hole assembly is retrieved by a special tool.

In a non-retrievable system, the bottom hole assembly (BHA) is not retrieved and after reaching the desired depth, the casing is cemented immediately. If the drilling process needs to continue, that bit is drilled with another drilling bit as a conventional casing drilling process. This is the most common and simplest method for casing drilling. Drillable PDC bits are used in non-retrievable systems.

Figure 8 shows retrievable and non-retrievable casing drilling bottom hole assemblies.

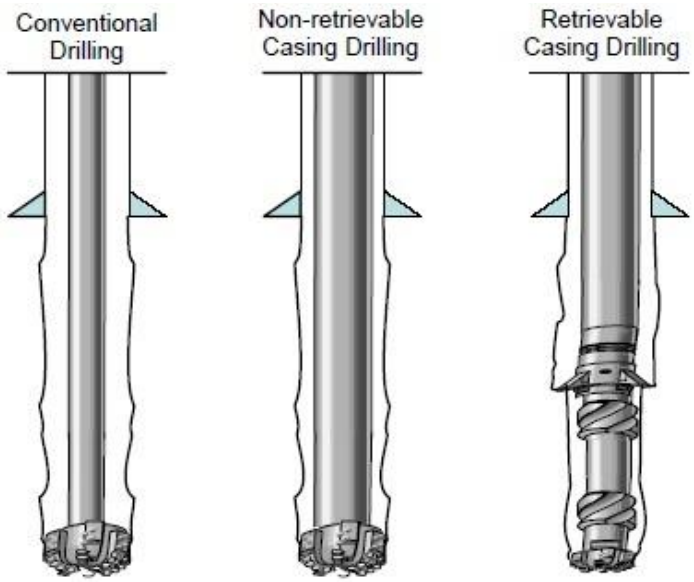

Figure 8. Differences between conventional drilling and retrievable and non-retrievable casing drilling assemblies (Robinson et al., 2008)

2.3. ADVANTAGES OF CASING DRILLING

Casing drilling has several benefits in mitigating wellbore stability problems and lost circulation situations. Thus, it is often chosen rather than a conventional drilling process. Casing drilling eliminates unexpected events that often accompany conventional drilling and its tripping problems. The most important benefits of casing drilling are given below:

2.3.1. No Tripping

There is no need to trip the drill string in casing drilling; the casing is at the bottom and ready to be cemented. This eliminates swab and surge pressures that accompany tripping operations.

2.3.2. Gauged Wells

In casing drilling, the annular clearance between the casing and the wellbore is much smaller than in conventional drilling. Consequently, a more circular and gauged wellbore is generated by the smoothing motion of the casing inside the well. According to Moellendick and Karimi (2011), the plastering/smear effect helps generate gauged wells by preventing break downs and wash outs inside the well. Figure 9 shows the differences between conventional and casing drilling wellbore shapes.

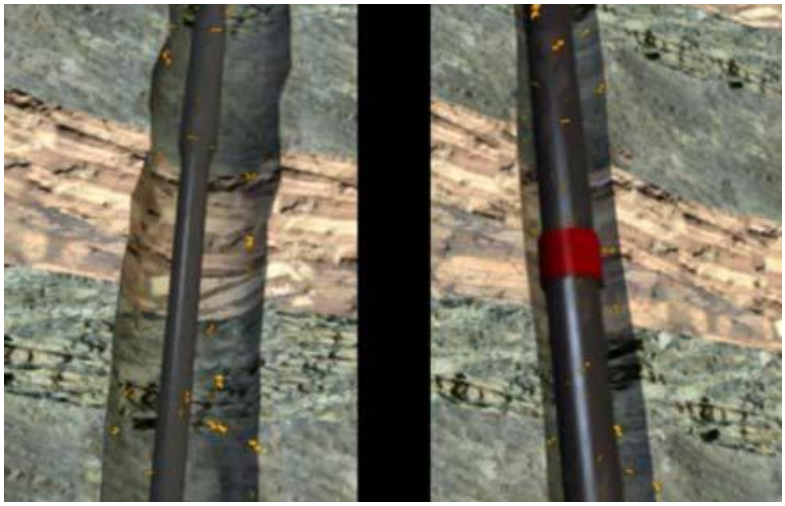

Figure 9. Differences between conventional drilling and casing drilling wellbore shapes (Moellendick and Karimi, 2011)

2.3.3. Reduce Drilling Times

Casing drilling reduces the total non-productive drilling times associated with tripping, running casing, and lost circulation problems. Lopez and Bonilla (2010) indicate that casing drilling reduces NPT by 30 % compared to conventional drilling. Figure 10 compares drilling days using casing drilling and conventional drilling in pressure depleted La Cira Infantas mature field, Columbia.

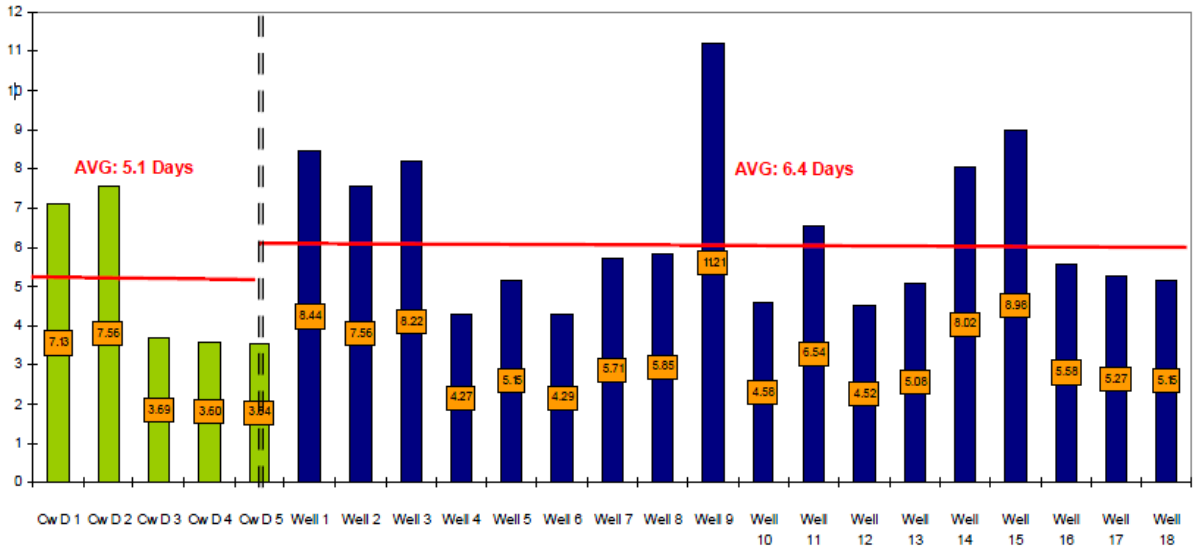

Figure 10. Drilling days between conventional drilling and casing drilling (Lopez and Bonilla, 2010)

2.3.4. Effective Borehole Cleaning

Casing drilling generates more effective borehole cleaning during drilling. The cuttings are circulated out with the high annular velocity that increases the borehole cleaning efficiency because of smaller clearance between the casing wall and the borehole wall. Consequently, stuck pipe problem do not occur. The small clearance between the casing and borehole is shown in Figure 11.

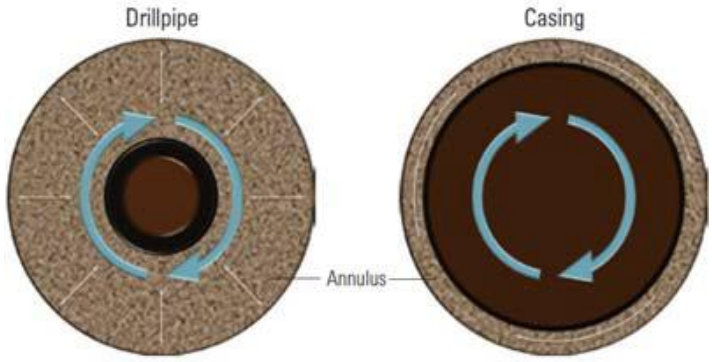

Figure 11. Differences between conventional drilling and casing drilling annulus size (Moellendick and Karimi, 2011)

2.3.5. Reduce Lost Circulation

Casing drilling with its plastering effect reduces lost circulation and improves wellbore stability. Fontenot et al. (2003) stated that lost circulation was eliminated by casing drilling in the Lobo Field in South Texas. Figure 12 shows the wells that had lost circulation which was eliminated by casing drilling.

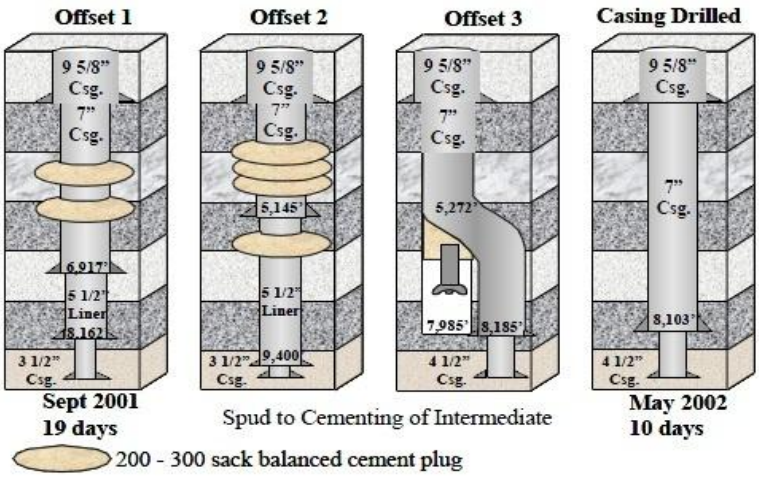

Figure 12. Casing drilling eliminates lost circulation (Fontenot et al., 2003)

2.3.6. Improve Well Control

In conventional drilling, well control problems often develop while tripping the drill string. In casing drilling, tripping is eliminated. For rig personnel, casing drilling rather than the conventional drilling is much safer. As a consequence, casing drilling enhances the well control and the Health, Safety and Environment (HSE).

2.3.7. Improve Production

Lost circulation damages production zones while drilling. Casing drilling prevents lost circulation and fluid invasion due to the plastering effect. This results in a better production rate than conventional drilling. Tessari and Warren (2006) state that casing drilling increased initial production rates and ultimate recovery in South Texas. Figure 13 compares seventeen conventional well production drilled in 2000 with twenty eight casing drilled wells in 2004.

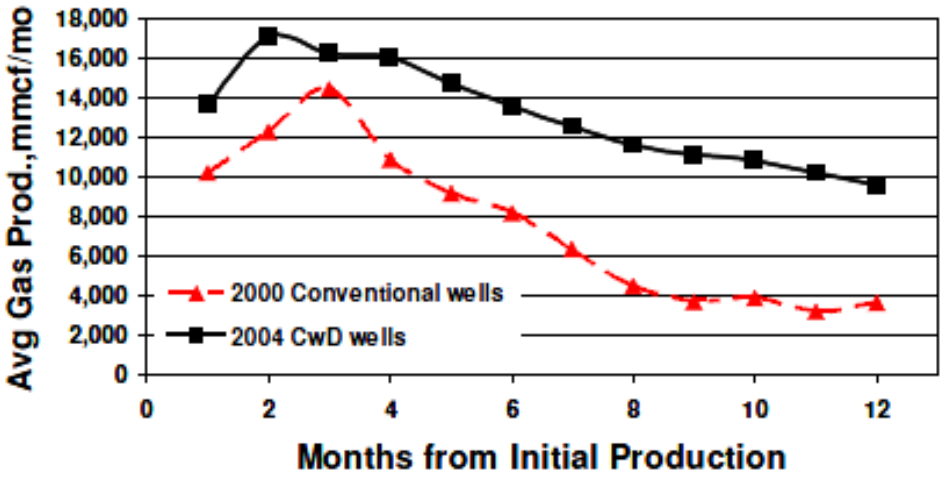

Figure 13. Comparison of production rate and decline between casing drilling and conventional drilling (Tessari and Warren, 2006)

2.3.8. Reduce Cost of the Wells

Casing drilling is generally applied to wells that have lost circulation and wellbore stability problems. Both in onshore and offshore drilling, daily rig costs are high and drilling problems are expensive. Since casing drilling eliminates or minimizes lost circulation and wellbore problems, the non-productive time is less. Figure 14 presents a comparison between casing drilling and loss circulation wells in cost/ft in depleted La Cira Infantas mature field in Colombia. Lopez and Bonilla (2010) stated that casing drilling reduced the cost of drilling by 10% compared to conventional drilling.

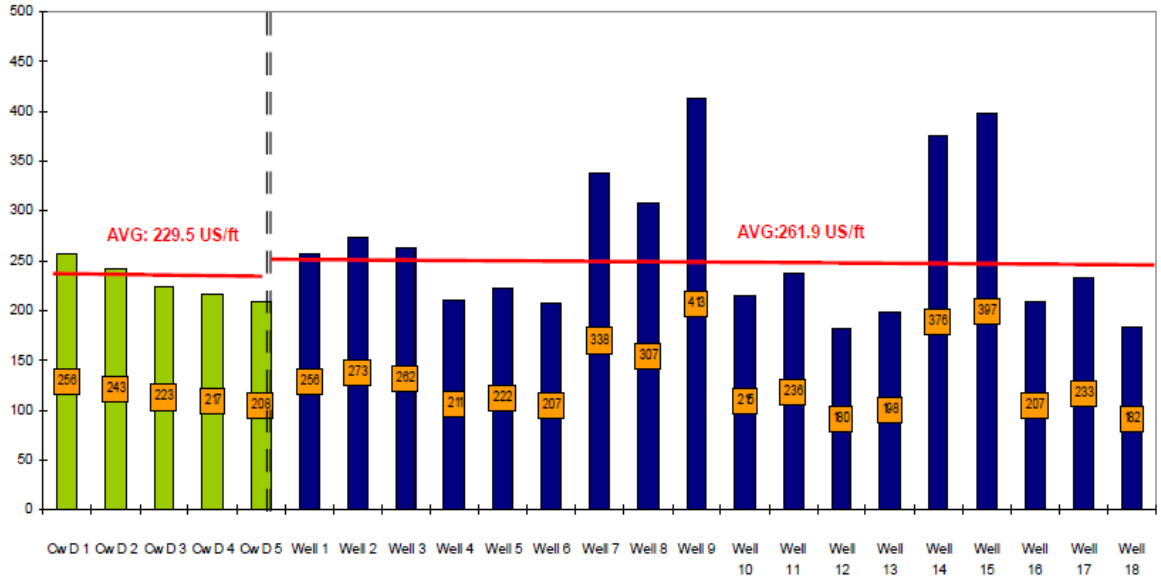

Figure 14. Comparison Cost/ft between casing drilling wells and loss circulation wells (Lopez and Bonilla, 2010)

2.4. SMEAR/PLASTERING EFFECT OF CASING DRILLING

In the smear effect phenomenon, mud particles from the drilling fluid and cuttings from the wellbore are embedded into the borehole wall. The casing rotates inside the wellbore with small clearance between the casing wall and wellbore wall. According to Lopez and Bonilla (2010), cuttings that are generated in casing drilling are finer grained

than conventional drilling cuttings because of casing rotation, side load forces, and high annular velocity. The cuttings and mud particles are smashed and pulverized into the small annulus resulting from casing rotation and become deposited in the borehole wall. This situation creates a natural seal in the pores which is much more efficient and impermeable than mud cake (2010). The cuttings from casing drilling are illustrated in Figure 15.

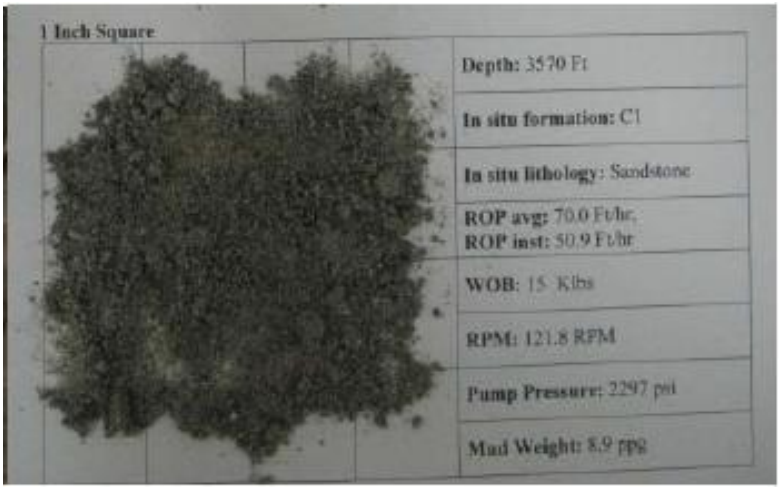

Figure 15. Cuttings size in casing drilling (Lopez and Bonilla, 2010)

Figures 16, 17, and 18 show the smear/plastering effect of casing drilling step by step.

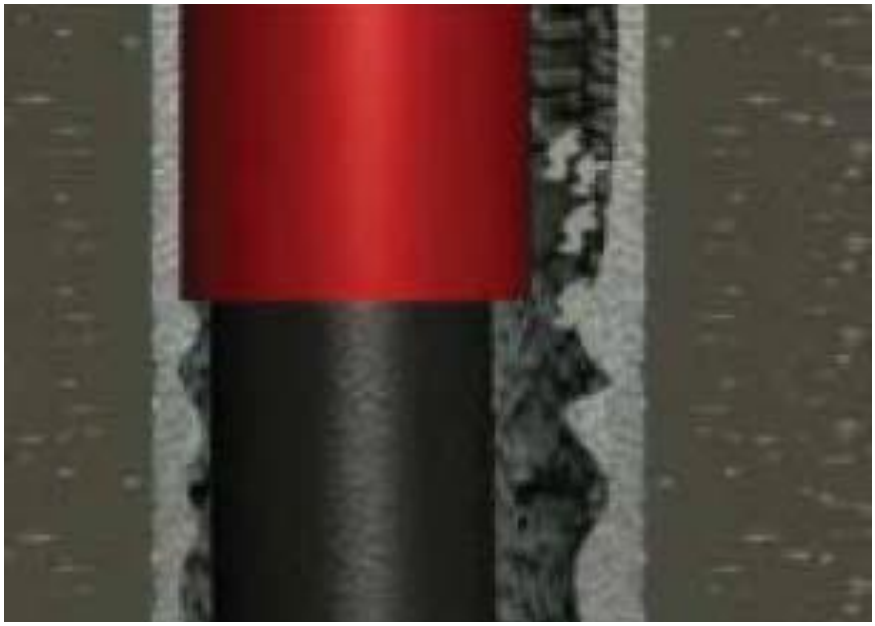

Figure 16. Casing is close to borehole and force the particles into wellbore wall (Moellendick and Karimi, 2011)

Figure 17. Impermeable mud cake is generated by smeared cuttings and mud particles (Moellendick and Karimi, 2011)

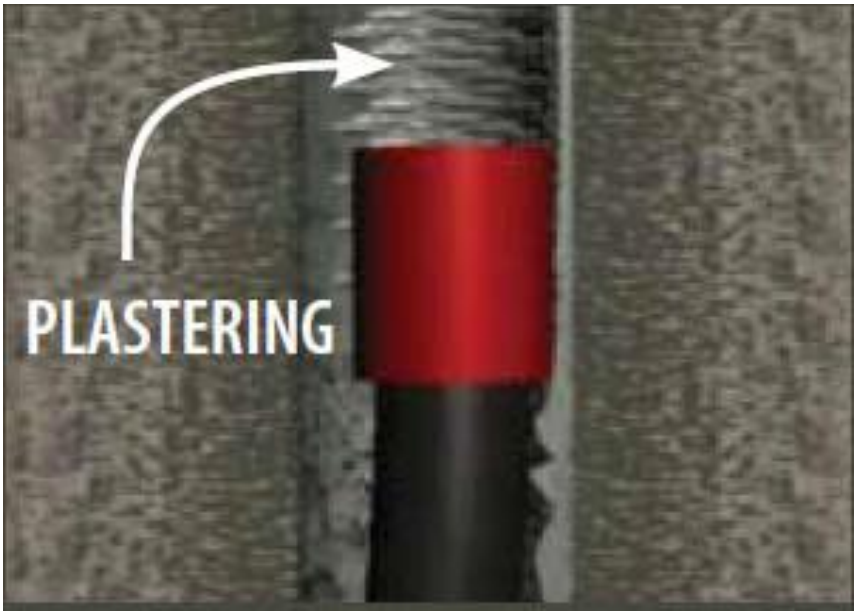

Figure 18. Natural seal is generated by plastering mechanism into the borehole wall by embedded mud particles and cuttings (Moellendick and Karimi, 2011)

A natural seal is achieved by the smear effect and fracture gradient is increased, so a wider window operation is achieved in depleted reservoirs (Moellendick and Karimi, 2011).

Moreover, the smear effect corresponds to the stress caging idea. When the cuttings and mud particles seal the fractures in the wellbore wall, stress caging results and this is the same as the smear effect in casing drilling.

Based on the stress caging idea, induced fractures are formed and lost circulation materials (LCM) are deposited close to the mouth of small induced fractures. Deposited solids make a bridge at the mouth and seal induced fractures at the wellbore wall. Consequently, the drilling fluid inside the crack dissipates into the formation and the pressure inside the crack becomes the same as the pore pressure of the formation. Therefore, fractures tend to close and fracture closure creates compression so that the

hoop stress at the formation gets higher than its original value (Alberty and Mclean, 2004). Figures 19 and 20 display the stress caging phenomenon and its applications.

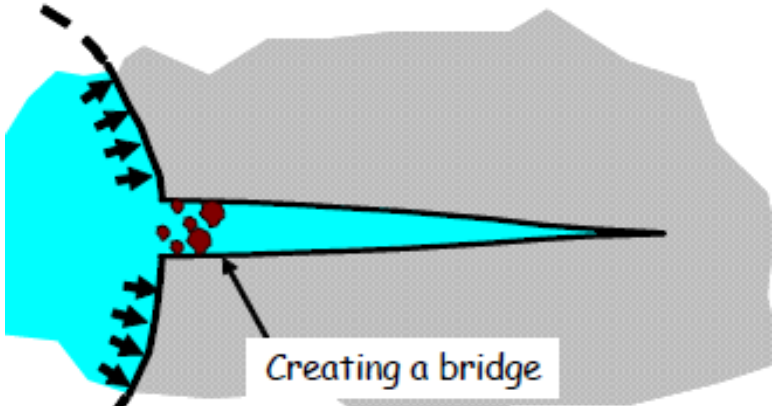

Figure 19. Stress caging and forming a bridge at mouth of an induced fracture (Alberty and Mclean, 2004)

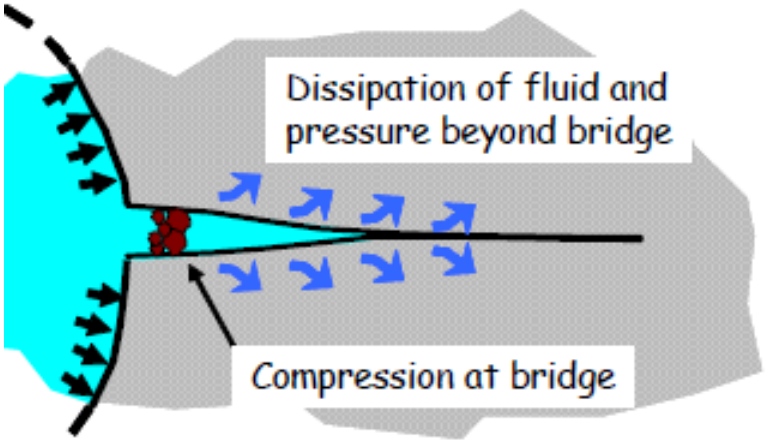

Figure 20. Fracture closure and dissipation of drilling fluid (Alberty and Mclean, 2004)

On the other hand, the fracture closure stress (FCS) application has a different approach compared to the stress caging. According to Dupriest (2005), widening the induced fracture width and keeping that fracture open with solid additives inside the

drilling mud is the main idea. The mud additives are not at the mouth of the fracture like stress caging, the particles are further inside the fractures. The important thing is keeping the tip isolated and final width must be enough to achieve fracture closure stress that is greater than the equivalent circulating density (ECD).

Both stress cage and fracture closure stress increase fracture gradient by increasing the hoop stress around the wellbore by propping fractures and sealing them with mud additives.

The smear effect in casing drilling is almost the same idea as stress caging because the particles make a bridge at the fracture mouth that seal and create an impermeable layer at the wellbore wall.

Furthermore, Watts et al. (2010) describes the smear in casing drilling in his article as;

> " The smear effect has been considered to be either a smearing and plastering of cuttings into the wellbore wall or the increase in hoop stress around the wellbore resulting when a crack is formed and particles are forced into the gap creating a wedge, thereby raising the effective fracture gradient."

Also, Fontenot et al. (2006), who were the first that mentioned smear effect, stated that the cuttings and mud particles become embedded into the borehole wall and create impermeable mud cake due to casing drilling forces, high annular velocity, pipe rotation and high equivalent circulating density (ECD). This impermeable mud cake creates a seal at the wellbore wall and prevents lost circulation at the depleted formations.

Additionally, as shown in Figure 11 previously, the clearance between the casing wall and wellbore wall is small and creates a smaller annulus area. Thus, the annular frictional pressure drop is higher than in conventional drilling, increasing the ECD. While a higher ECD may not be desirable in conventional drilling because drilling fluid leaks

off, a higher ECD is beneficial in casing drilling since the higher ECD generates small, tiny fractures at the wellbore wall. Because of higher ECD and pipe rotation, the mud particles and cuttings are pulverized in the annulus and smeared at fracture mouths, making a bridge and plugging pore throats, as in stress caging (Karimi et al., 2011).

Another important benefit of casing drilling is the smoothing effect of eccentric rotation of the casing string. This smoothing and eccentric motion achieves a more circular wellbore shape than conventional drilling. This motion also helps develop an impermeable mud cake and the mud cake damage is less than in conventional drilling. Thus, smooth and eccentric casing motion improves wellbore stability compared to conventional drilling. Figure 21 shows the eccentric motion of casing string while casing drilling.

All in all, the smear effect has lots of advantages in preventing lost circulations and creating a gauged hole.

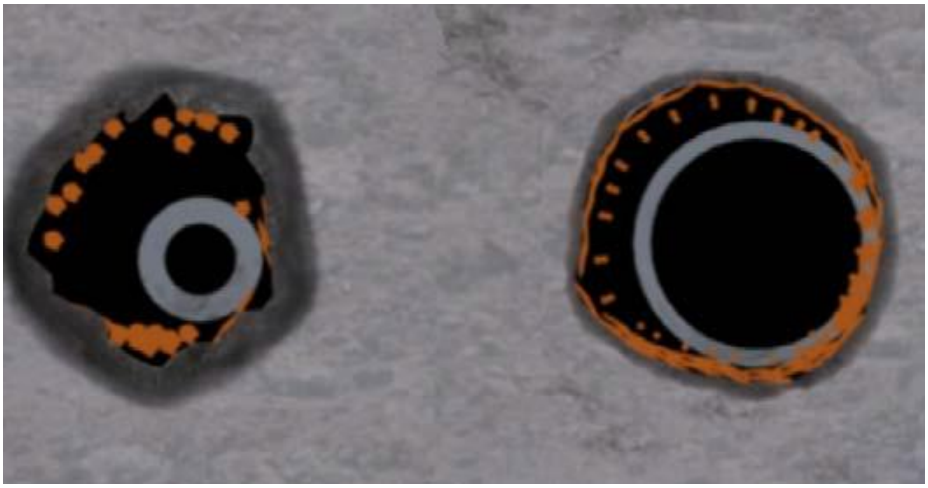

Figure 21. Eccentric motion of casing strings (right) compare to conventional drill strings (left) (Moellendick and Karimi, 2011)

3. Finite Element Modeling of Smear Effect in Casing Drilling Operations

3.1. FINITE ELEMENT MODELING

There are many finite element method programs that have been used to simulate problems encountered in petroleum industry. In this study, ABAQUS/CAE is used to simulate fractures in casing drilling applications. .

In this chapter, the basic concepts and descriptions of a finite element model are given. The model geometry, load types, boundary conditions, physical properties of material, mesh properties and extended finite element method (XFEM) are discussed and presented.

3.1.1. Plane Stress and Plane Strain

Plane stress elements generally are used where the thickness of the material or plane is very small relative to its lateral directions. One of the principal stresses σ_x, σ_y, σ_z is zero as is seen in thin or flat materials. Plane stress elements are defined in X-Y coordinates (Abaqus 6.10 EF, Analysis User's Manual, 2010).

On the other hand, plane strain elements can be used if the one dimension of the material is very large relative to other dimensions. In general, the Z direction is very large compared to X and Y directions when modeling a vertical wellbore. It is assumed that the principal strain in the Z direction is zero (Abaqus 6.10 EF, Analysis User's Manual, 2010).

In this study, the model is used in two dimensions rather than three. For a vertical wellbore and very large Z dimension compared to the X and Y direction; plane strain conditions are used in the model.

3.2. GEOMETRY OF THE FINITE ELEMENT MODEL

In general, rock mechanics and fracturing problems are three dimensional. However, two dimensional modeling can be used as a beginning. Plane strain elements are used because there is no displacement and shear stress along the wellbore direction.

First, a model was created to open cracks in extended finite element method (XFEM); and a wellbore is generated in a square domain. Figure 22 shows the base geometry. The wellbore diameter is 8 inches and the lengths of the domains are ten times larger than the wellbore diameter that is 80 inches in length and width. 8 different regions exist close to the wellbore which dimensions are same with the radius of the wellbore and these regions are enriched in the extended finite element model. The cracks are created in these enriched regions that are 4 inches close to the wellbore wall.

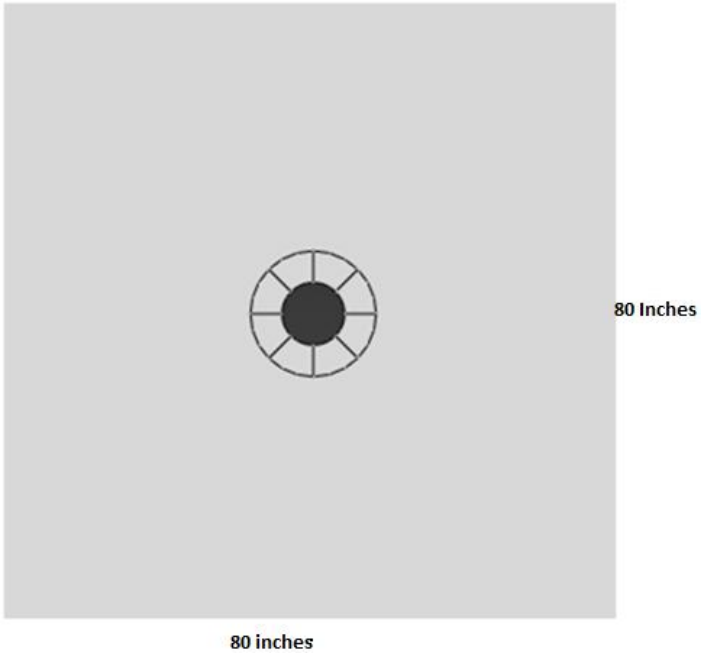

Figure 22. Geometry of the base finite element model

The base model is two dimensional planar which is deformable, and it is placed in the X-Y plane. The deformable parts change shape under applied loads and stresses.

Also, another model geometry to open cracks and seal them is a quarter of the square, because of model symmetry. This model is the same as the previous one, which is two dimensional planar and deformable in the X-Y plane. In this model, wellbore radius (r_w) is the same as the previous one which is equal to 4.25 inches. Width and length of the model is also 40.25 inches in the X and Y directions. In this model, the left hand edge represents a plane of symmetry. That is, there is no normal displacement allowed and no tangential or shear stress applied. Furthermore, for some loadings a symmetry condition will also be used along a portion of the top boundary. In Figure 23, the quadrant model of the wellbore is shown.

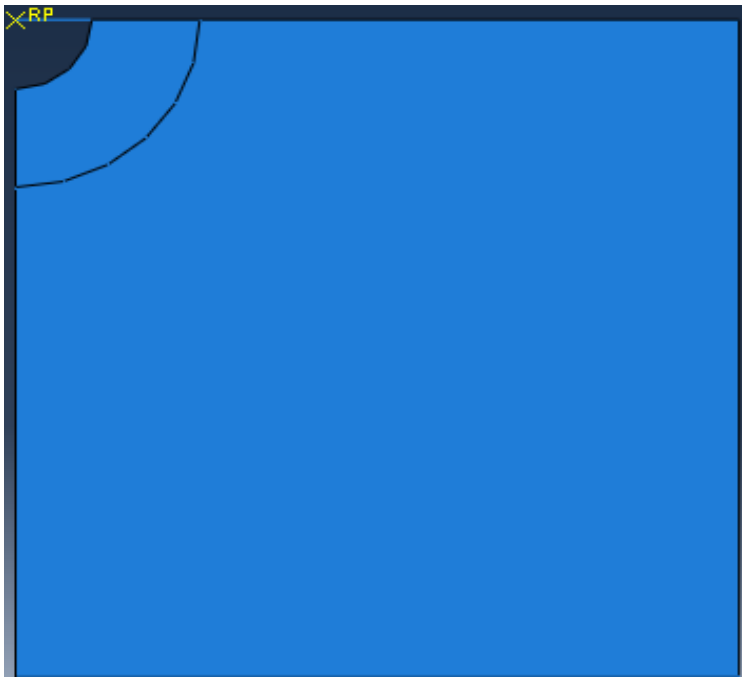

Figure 23. Quadrant geometry of wellbore in finite element analysis

3.3.FORMATION IN SITU PRINCIPAL STRESSES

Three mutually perpendicular principal in situ stresses exist at any depth of the earth's formation. These principal stresses are seen in Figure 24.

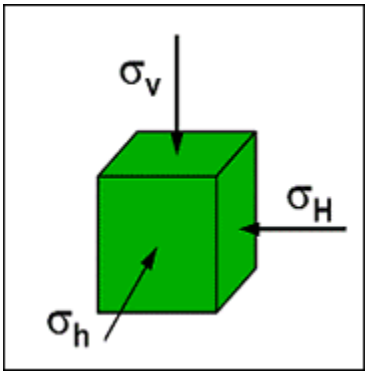

Figure 24.Formation in situ principal stresses

In general, maximum principal stress σ_v is the vertical principal stress that is equal to overburden stress into the formations. The other principal stresses are horizontal and these are maximum horizontal (σ_H) and minimum horizontal (σ_h) stresses that are seen in Figure 24.

In this study, it is assumed that the horizontal in situ, far- field stress components are not equal. Different ratios of maximum and minimum horizontal stresses are used along with plane strain. Thus, overburden stresses are not included. Figure 25 shows the general stress components of the model. As a stress anisotropy, $S_{min}=S_{max}$, $2S_{min}=S_{max}$, and $3S_{min}=S_{max}$ are used to see the effects of horizontal stress ratios.

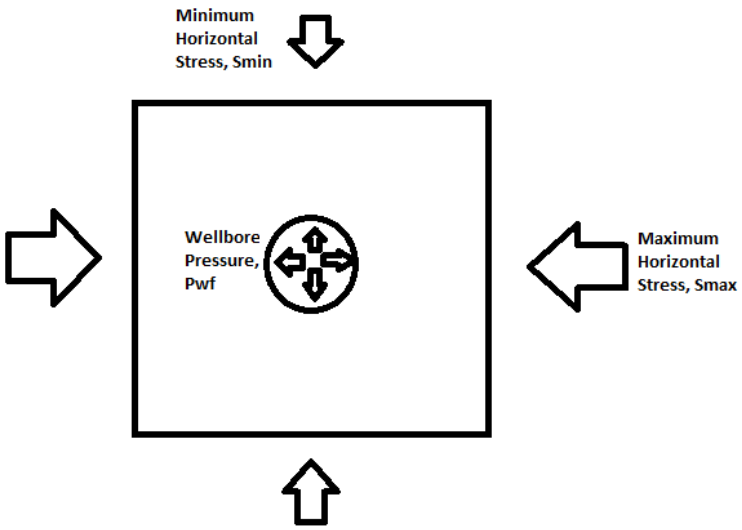

Figure 25. Horizontal stress components of the model

3.4.FRACTURE MECHANICS

Fracture mechanics investigates crack initiation, crack propagation and crack evaluation in materials. In general, there are three types of rock failures; tensile, compressive and shear. Fractures are tensile failure in general and lost circulation tends to be due to the tensile failure of the rock. Fracture mechanics of a crack initiation and propagation were modeled by the extended finite element method (XFEM) to initiate and propagate the crack in 3.4.4.

3.4.1. Fracture Initiation

A crack starts to initiate when applied stresses are higher than the material's strength, and if the stresses are high enough, the material breaks. According to Dupriest (2005), to open a crack into a formation, the pressure applied to the formation needs to be high enough to overcome the rock strength and stresses inside the rock.

In oil field application, the leak-off test is used to estimate the minimum far field stress and maximum pressure that the formation can stand. Figure 26 shows the leak-off graph.

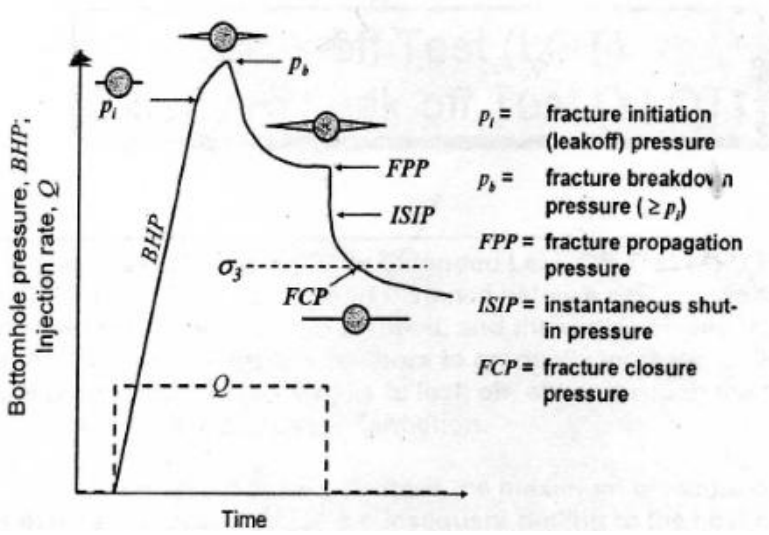

Figure 26. Leak-off test (Hawkes et al., 2005)

In Figure 26, a bottom hole pressure (BHP) vs time graph is used to illustrate fracture initiation, fracture breakdown, fracture propagation, fracture closure pressure and instantaneously shut-in pressure. Initially, bottom hole pressure increases linearly until fracture initiation pressure is reached. In theory, this is the pressure at which tangential stresses around the borehole overcomes the tensile strength of the rock. At fracture initiation pressure, small and tiny fractures are initiated but there is no lost circulation at that pressure. After that, with increasing pressure, the formation breaks down and wider fractures are formed. Drilling fluid penetrates into the formation. This is called the formation breakdown pressure. In general, this pressure is equal to the minimum horizontal stress at that time. If injection or pressure increases, fractures propagate by

injection and lost circulation takes place at the fracture propagation pressure. After the pump is stopped, the pressure decreases to the instantaneous shut-in pressure.

3.4.2. Fracture Propagation

Fracture propagation starts when pressure or flow rate keeps increasing after fracture or crack initiation.

Two types of fracture propagation criteria are exist; one based on stress and the other based on energy. In extended finite element modeling, the stress criteria are used to initiate and propagate fractures.

In this study of fracture mechanics, the stress at the tip of any crack is assumed to be infinite. Thus, the value of the crack tip stress cannot be used as a fracture criterion. A measure of the severity of the stress field in the material in the immediate neighborhood of the crack tip is called the stress intensity factor. The critical value of the stress intensity factor at which the crack starts to grow is a material property and is determined experimentally. This value is also referred to as the fracture toughness of the material.

3.4.3. Fracture Types

Three different modes of crack initiation exist based on their relative body motions; opening, in-plane shear, and out of plane shear modes. These fracture types are shown in Figure 27.

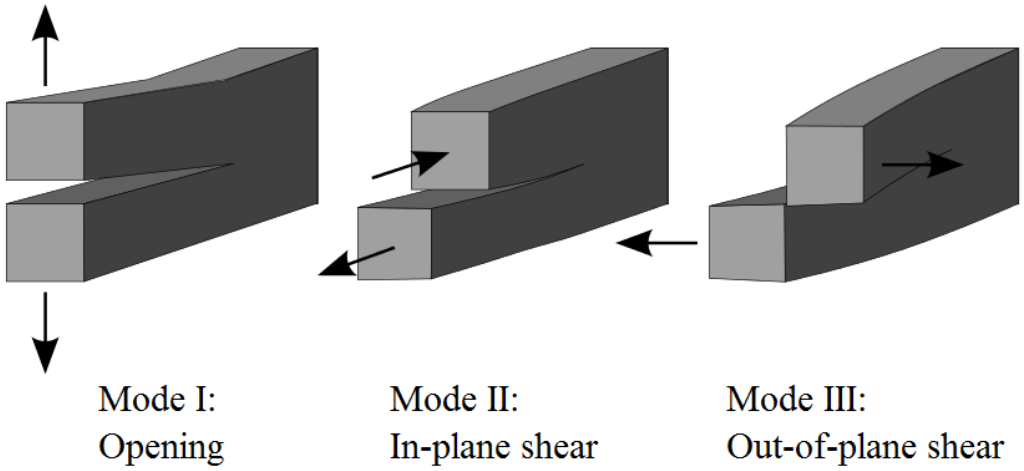

Figure 27. Different modes of fractures

A mode I opening crack is a tensile failure. Generally, fractures are mode I when tensile strength is exceeded. Mode II and mode III cracks are shear failures. Mode II is sliding mode and mode III is tearing mode. In mode II, the loading is parallel to the crack plane and perpendicular to crack front. In mode III, loading is both parallel to the crack front and crack plane.

In this study, mode I opening as a tensile failure of the formation is used. In regions of excessively large compressive stresses, the formation may experience mode II or mode III failures, but this is quite rare.

3.4.4. Extended Finite Element Method (XFEM)

In this study, extended finite element modeling is used to generate multiple cracks in a single wellbore. By generating multiple cracks, the near wellbore stresses and effects on the near wellbore region can be studied.

In XFEM, the crack initiation and propagation along an arbitrary path can be studied. It is not necessary to define the crack propagation trajectory. The trajectory is

solution dependent and XFEM determines the arbitrary path. Also, crack domain and initial crack location can be specified in the XFEM analysis.

The crack domain when the cracks are initiated and propagated is specified in the model to initiate and propagate the cracks. On the other hand, initial crack location can be specified, but this was not done and ABAQUS determines crack location by principal stresses that are greater than the maximum defined in traction separation laws. Figure 28 shows the crack domain and location in 2-D and 3-D.

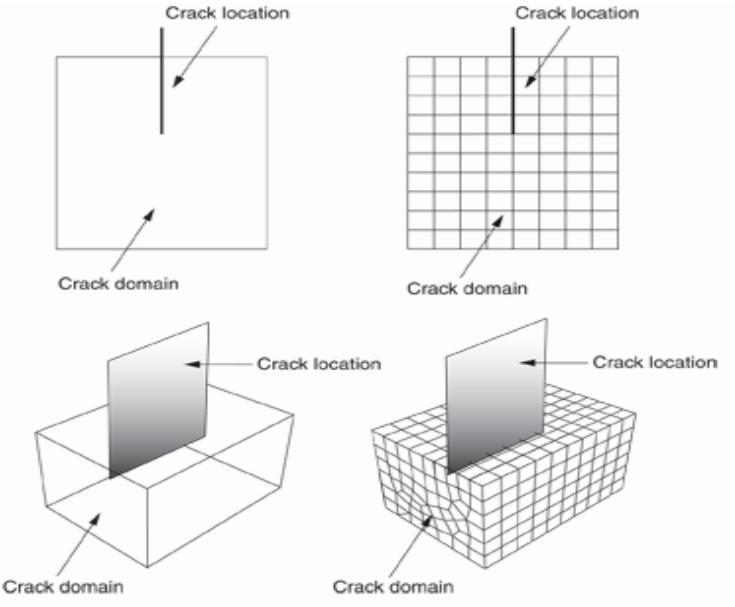

Figure 28. Crack domain and location in XFEM (ABAQUS/CAE User's Manual, 2010)

Traction-separation cohesive behavior is used to simulate crack initiation and propagation. In traction-separation cohesive behavior, linearly elastic traction-separation takes place before damage occurs. Damage evolution and damage initiation are related to material properties and specified in the traction-separation behavior. The elastic behavior can be written in terms of an elastic constitutive matrix that includes normal and shear stresses.

$$\mathbf{t} = \begin{Bmatrix} t_n \\ t_s \\ t_t \end{Bmatrix} = \begin{bmatrix} K_{nn} & 0 & 0 \\ 0 & K_{ss} & 0 \\ 0 & 0 & K_{tt} \end{bmatrix} \begin{Bmatrix} \delta_n \\ \delta_s \\ \delta_t \end{Bmatrix} = \mathbf{K}\boldsymbol{\delta}.$$

The nominal traction stress vector, t, has three components reflecting the normal and two shear tractions. The separations are represented by δ_n, δ_s, and δ_t. The terms K_{nn}, K_{ss}, and K_{tt} are calculated for the enriched region and specify the elastic stiffness and traction-separation behavior (ABAQUS/CAE User's Manual, 2010).

In XFEM, it is necessary to define the enriched region and its properties to generate cracks in this region. The crack can initiate and propagate in the enriched region by solution dependent and arbitrary crack trajectory. Also, the enriched radius in XFEM can be specified.

In this study, the maximum principal stress principal is used when modeling multiple cracks. This can be represented by;

$$f = \left\{ \frac{\langle \sigma_{\max} \rangle}{\sigma^{o}_{\max}} \right\}$$

$\sigma^{o}_{\max}$ = maximum allowable principal stress

The symbol $\langle\ \rangle$ represents the Macaulay bracket and its interpretation is, $\sigma_{\max} = 0$ if $\sigma_{\max} < 0$ and $\langle \sigma_{\max} \rangle = \sigma_{\max}$ if $\sigma_{\max} \geq 0$. As a result, the damage initiation starts when the ratio is equal to one (ABAQUS/CAE User's Manual, 2010).

For damage evolution, the rate of degradation is specified when initiation criteria have occurred. A damage variable, D, shows the damage between crack surfaces and edges of crack elements. Its value is zero at the beginning. It starts to increase and

reaches a value of 1 after damage initiation. The stress components are affected by the damage in the elements and these normal shear stress components are;

$$t_n = \begin{Bmatrix} (1-D)T_n \\ T_n \end{Bmatrix}, T_n \geq o$$

$$t_s = (1-D)T_s$$

$$t_t = (1-D)T_t$$

where T_n, T_s, and T_t are the normal and shear stress components predicted by the elastic traction-separation behavior for the current separations without damage (ABAQUS/CAE User's Manual, 2010).

The important aspects of the XFEM feature are that the user does not have to specify the location of a crack and the crack does not have to follow element boundaries.

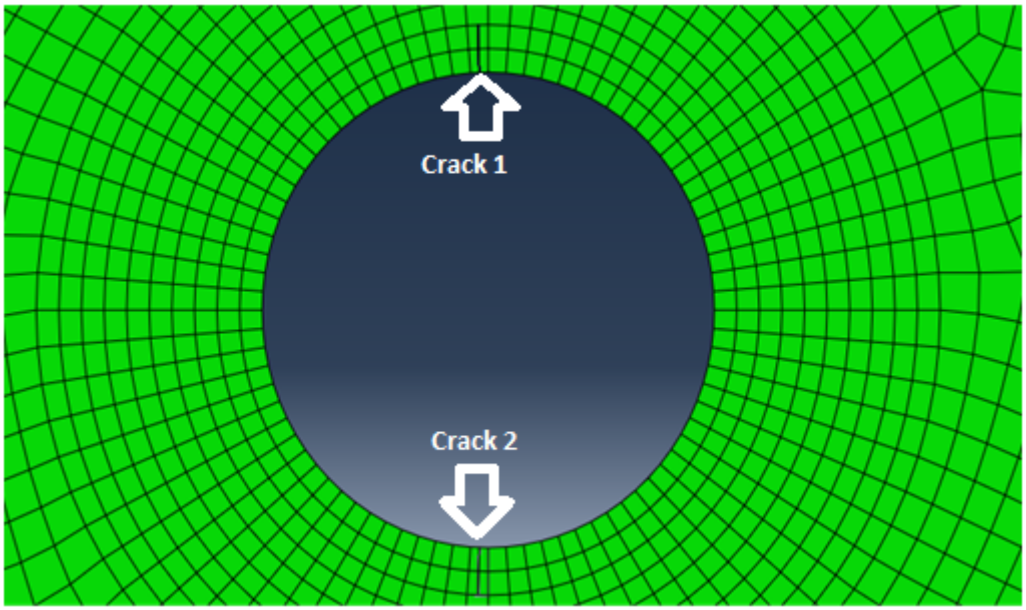

Figure 29. Example of multiple cracks by using XFEM in ABAQUS

In conclusion, extended finite element modeling is a way to analyze crack behavior as an enriched region. It is a very effective way to model crack initiation and propagation along an arbitrary and solution-dependent crack trajectory. In this study, multiple crack behavior is analyzed by using extended finite element modeling to study wellbore stress distribution along the wellbore wall by investigating a single crack and multiple cracks.

3.5. Loading, Initial, and Boundary Conditions of Finite Element Model

Loading, initial and boundary conditions are needed for ABAQUS to simulate crack behavior and sealing effects. Information is given below about the loading types, initial conditions, and boundary conditions of finite element modeling.

3.5.1. Loading Conditions

Loading conditions are applied to the model in steps as static linear perturbation and steady-state dynamic. Pressures are applied normal to the surfaces of the model. Also, two ways exist to specify distributed loads: element-based and surface-based distributed loads. Element-based distributed loads are applied on element bodies, surfaces and edges. Surface-based distributed loads are applied on geometric surfaces and edges. Here surface-based distributed loads are used (ABAQUS/CAE User's Manual, 2010).

In the models, pressures are applied as minimum horizontal stress, maximum horizontal stress and wellbore pressure inside the well. These loads are applied to the surfaces and are distributed uniformly over surfaces. The magnitudes are force per unit area.

Pore fluid flow in the model is coupled pore fluid diffusion/ stress analysis. In pore fluid flow, seepage coefficients can be defined on element faces or surfaces. It is an outward normal flow velocity directly at nodes, element faces and surfaces. Pore fluid

flow is used in the consolidation step analysis and there is a flow from the interior region of the model to its exterior region. In pore fluid flow, a proportion to the difference exists between the current pore pressure and reference pore pressure value (ABAQUS/CAE User's Manual, 2010).

$$v_n = k_s(u_w - u^{\infty}_w)$$

where

v_n = component of the pore fluid velocity in the direction of the outward normal to the surface

k_s = seepage coefficient

u_w = current pore pressure at this point on the surface

u^{∞}_w = a reference pore pressure value.

When there is a difference between the formation pore pressure and current pore pressure at the wellbore surface, seepage exists by proportionally. By using pore fluid flow, seepage can take place and affects stress distribution around the wellbore wall. Pore fluid flow is used to see the effects of leak off of drilling fluid into the formation.

3.5.2. Initial and Boundary Conditions

Initial and boundary conditions are specified at elements or nodes in ABAQUS. In general, initial conditions are prescribed conditions that can be provided manually in an external input file or by a user's subroutine. In this model, initial conditions are directly written in external input files. If initial conditions are not specified, they are assumed zero by ABAQUS and all the calculations are done using these assumptions. In this study, void ratio and pore pressure are taken as initial conditions and these are all specified as inputs.

Initial void ratio is one of the initial conditions. Void ratio can be defined as ratio of the volume of void to the volume of solid parts in a porous medium (ABAQUS/CAE User's Manual, 2010). Moreover, another initial condition of the model is initial pore pressure. Pore pressure is the hydrostatic fluid pressure inside the pores of formations that can support the overburden of the rocks above the formations. In general, reservoirs are normally pressured and the pore pressure is equal to the hydrostatic pressure of a water column and overburden at a certain depth. On the other hand, in depleted reservoirs, pore pressure of a formation is smaller than the expected pressure and the pressure has decreased below the pressure of the adjacent zones in the main reservoirs. In this study, the initial pore pressure is defined as pore pressure of the model and defined to model a fluid filled porous medium.

Boundary conditions are the properties than can be used when simulating in ABAQUS and these conditions are the values of all basic solution variables at certain nodes. There are different kinds of boundary conditions and displacement, rotation, pore pressure types of boundary conditions are used. In stress/displacement analysis, the symmetry boundary conditions can be used. Boundary conditions regulate the degrees of freedom in the model. For example, for an x- symmetry boundary condition, there is symmetry about a plane that has restrictions in the X direction. Movement in the X direction is zero and also, the rotation degree of freedom is also fixed. (U_1, UR_2, UR_3=0). The other symmetry boundary conditions and degrees of freedom are seen below (ABAQUS/CAE Analysis User's Manual, 2010).

XSYMM Symmetry about a plane X=constant (degrees of freedom 1, 5, 6=0).

YSYMM Symmetry about a plane Y=constant (degrees of freedom 2, 4, 6=0).

ZSYMM Symmetry about a plane Z=constant (degrees of freedom 3, 4, 5=0)

Since the model is a quatrant in two dimensions, x-symmetry and y-symmetry as boundary conditions are applied. To create sealing a velocity boundary condition at the sealing location is used. Thus, at the sealing location, velocity to the Y direction is equal to zero and this situation creates a sealing point to achieve the smearing effect. For the XFEM, displacement boundary conditions are applied. The X and Y direction movements are fixed to prevent model movement and also, the third degree of freedom is fixed as a rotation boundary on the X and Y axis. Figure 30 shows an example of loading and boundary conditions in this study.

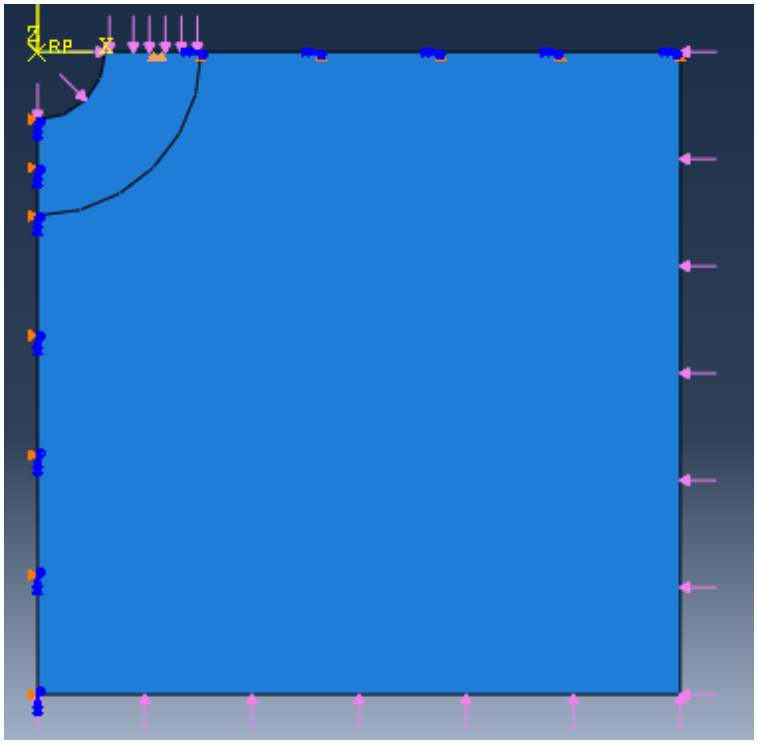

Figure 30. Example of loading and boundary conditions in ABAQUS

3.6.Meshing of Finite Element Model

Meshing of the finite element model generates meshes on parts and assemblies to control model analysis. By mesh module controls in ABAQUS, mesh density at local or

global parts, element types of meshes, and element shapes can be controlled. There are two types of mesh generation; top-down meshing and bottom-up meshing.

In top-down meshing, meshes are generated by going down from the parts or nodes and elements region. Furthermore, the mesh adapts accurately with the geometry of a region in the top-down meshing technique. In one, two or three dimensional parts, top-down meshing can be used. An example figure for top-down meshing is shown in Figure 31 and shows the mesh adaptation with parts of the geometry.

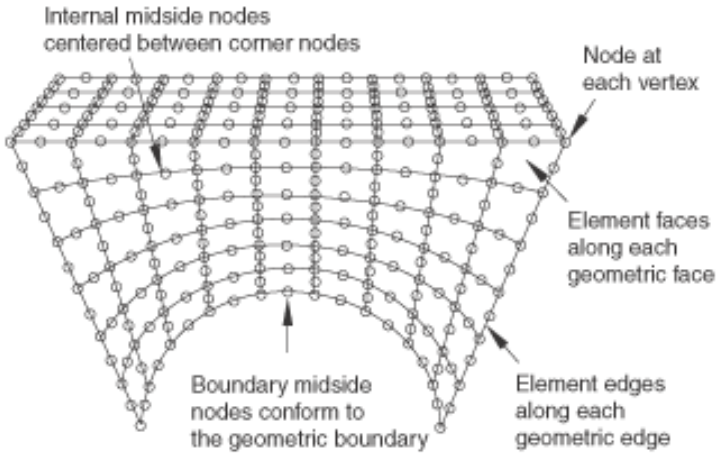

Figure 31. Mesh adaptation to the geometry in top-down meshing technique (ABAQUS/CAE User's Manual, 2010)

In bottom-up meshing, meshes are generated by going up from two dimensional entities to create three dimensional meshes. Only three dimensional part geometry is available in bottom-up meshing (ABAQUS/CAE User's Manual, 2010). In this model, a top-down meshing is used for two dimensional parts of the model. In top- down meshing, three different techniques exist to generate element shapes. These are structured meshing, swept meshing and free meshing. The structured meshing technique has control over the

mesh patterns to particular model shapes, like square or rectangular. The swept meshing technique is the same as the structured meshes to control mesh patterns to particular model shapes, but is only generated at an edge or a face. Free meshing is less controlled and there is no exact pattern for the mesh. Mesh pattern cannot be estimated (ABAQUS/CAE User's Manual, 2010). In this study, structured and free mesh techniques are used to analyze the smearing effect.

Ouad elements are used to assign mesh control for element shapes. There are three types of element shapes for two dimensional models: quad, quad dominated; and triangular elements. Quadrilateral element shapes are convenient because there are no triangle elements in meshing design that can distort the model.

Also, plain strain and pore fluid/stress element types are used for mesh element types. For plain strain elements, four node bilinear plain strain quadrilateral elements (CPE4) are used, and four node plain strain quadrilateral, bilinear displacement, and bilinear pore pressure (CPE4P) are used for pore fluid/stress element types. Their geometric orders are all linear and elastic. Figures 32 and 33 show the meshing of the models. Figure 32 meshes are all generated structured technique and quadrilateral element shapes and plain strain element types. Figure 33 shows the free and structured mesh techniques. They are plain strain element types, and quad element shapes.

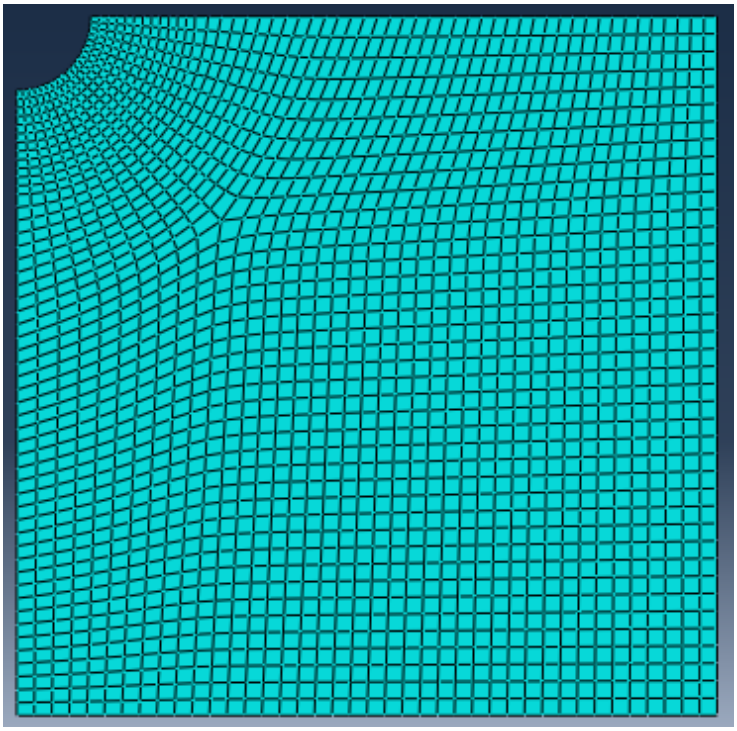

Figure 32. Example of structured mesh techniques and quadrilateral element shapes

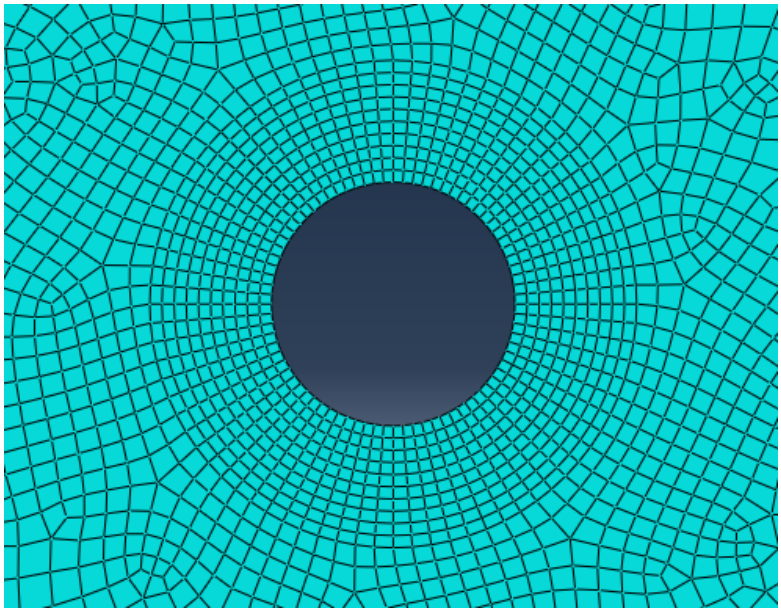

Figure 33. Example of structured mesh and free mesh techniques

3.7. STEPS OF FINITE ELEMENT MODEL

In ABAQUS, a step procedure is used to analyze the sequence of one step or more steps in a specific amount of time. The series of steps generate a convenient way to apply changes as changing loading and boundary conditions, interactions between the parts, and different kinds of changes that are seen in the model (ABAQUS/CAE User's Manual, 2010).

There are two main types of steps that are used in ABAQUS finite element modeling, initial steps and analysis steps. The initial step is the first step sequence of the model and it helps to define loading, boundary conditions, interactions at the very beginning of the analysis. On the other hand, analysis steps follow and can be done during certain steps. In analysis step, static stress analysis, soil analysis or geostatic analysis can be done and they can come after different kinds of steps in the procedure (ABAQUS/CAE User's Manual, 2010).

Two main procedure types exist; general and linear perturbation procedures. In this study general procedures are used and general static procedure is used; geostatic and soil steps procedures are used as sub divisions of general procedures. In a general analysis step, nonlinearities can be included in the model and the beginning condition of each general step is the ending conditions for the last general step.

In static stress analysis that is a subdivision of general step procedure, inertia effects can be neglected and also the model can be linear or non-linear. It also neglects material deformation which is related to time.

In stress analysis for fluid-filled porous materials, the soil step is used and a coupled pore fluid diffusion/stress analysis can be performed to simulate single phase, fully saturated or partially saturated porous materials. Pore pressure elements are applied in stress analysis in porous media and all the properties of pore fluid flow are defined.

Also, stress analysis in porous material can be linear or non-linear and can be transient or steady-state (ABAQUS/CAE Analysis User's Manual, 2010).

In general, partially and fully saturated flow is modeled in pore fluid stress analysis. Partially saturated flow occurs as the wetting fluid is absorbed in the porous media by capillary pressure. In fully saturated flow, the porous medium is fully saturated by fluid and consolidation analysis is used for fully saturated flow (ABAQUS/CAE User's Manual, 2010). In this study, fully saturated flow is used to model pore fluid/stress analysis.

There are two analyses in the soil step: steady-state analysis and transient analysis. In steady state analysis, it is assumed that no transient effects are seen in the model and there is a constant velocity. Also volume is constant for fluid per unit volume in the material. Thus, analysis of the model is steady state and all the dynamic parameters are constant. On the other hand, in transient analysis, the system becomes transient and after some time it becomes unconditionally stable. As a result, transient soil analysis ends when it reaches steady-state conditions or when it completes a specific time period (ABAQUS/CAE User's Manual, 2010).

In soil step analysis, the permeability must to be defined. Permeability defines the relationship between volumetric flow rate per unit area of a fluid through a porous material and the gradient of the effective fluid pressure. In ABAQUS, permeability is defined as hydraulic conductivity and its unit is LT^{-1}. In the Darcy equation, permeability's unit is L^2 so unit conversation needs to be done. Permeability can be isotropic, anisotropic and orthotropic (ABAQUS/CAE User's Manual, 2010). In this study, isotropic permeability is used with a constant value everywhere in the model.

The other step used in the models is the geostatic step. In geostatic stress field procedure, the stress fields come into equilibrium with various applied loads and

boundary conditions in the model. Pore pressure elements are used and this is the first step for the geotechnical analysis. In general, after the geostatic step, the soil step is used to perform pore fluid flow analysis. In the geostatic step, it is usually geometrically linear and it is better to get initial equilibrium in the linear step in the model (ABAQUS/CAE User's Manual, 2010). In this study, geostatic step is the first step to get equilibrium in various loads and boundary conditions. After the geostatic step, the soil transient steps are used.

3.8. MODEL INPUTS

Table 1. Model inputs for extended finite element model (XFEM)

Model Inputs for XFEM	Values	Units
Length	80	Inches
Width	80	Inches
Radius	4	Inches
Young Modulus (E)	1090000	Psi
Poisson's Ratio (υ)	0.225	
Density	0.095	Lb/in^3
Minimum Horizontal Stress (S_{min})	3000	Psi
Maximum Horizontal Stress (S_{max})	$2S_{min}$, $3S_{min}$	psi
Wellbore Pressure (P_{wf})	variable	psi
Maximum Principal Stress Criterion (Maxps)	3000	Psi
Damage Evolution Type	Energy	
Damage Evolution Softening	Linear	
Damage Evolution Degradation	Maximum	
Damage Evolution Mixed Mode Behavior	BK law model	
Damage Evolution Mode Mix Ratio	Energy	
Damage Evolution Power	1	
Normal Mode Fracture Energy	16	Lbf/in
Shear Mode Fracture Energy First Direction	16	Lbf/in
Shear Mode Fracture Energy Second Direction	16	Lbf/in
Damage Stabilization Cohesive Viscosity Coefficient	0.00001	

Table 2. Parameter for a quadrant model with and without pore pressure

Parameter	**Values**	**Units**
Length	40.25	Inches
Width	40.25	Inches
Radius	4.25	Inches
Young Modulus (E)	1090000	Psi
Poisson's Ratio (υ)	0.225	
Density	0.0979	Lb/in^3
Minimum Horizontal Stress (S_{min})	3000	Psi
Maximum Horizontal Stress (S_{max})	$2S_{min}$, $3S_{min}$	psi
Wellbore Pressure (P_{wf})	6000	psi
Pressure After Bridge ($P_{afterbridge}$)	3000	Psi
Pressure Before Bridge ($P_{beforebridge}$)	6000	Psi
Pressure inside the Fracture (P_f)	6000	Psi
Fracture Length	6	inches
Initial Pore Pressure	3000	psi
Pore Fluid Flow Velocity	0.7 and 3	in/min
Permeability	100	md
Hydraulic Conductivity	0.0023	in/min
Void Ratio	0.3	

4. Results of the Finite Element Models

In this chapter, results from the finite element models are discussed and stress analyses are done for different types of models such as; no porous fluid in the model; with porous fluid in the model; and porous fluid flow in the models. All the results and different aspects of the models are calculated and compared to illustrate effects of different parameters.

4.1. Results and Discussion Without Porous Fluid In the Model

In this part, the model is generated without porous fluid inside and stress analysis is done at the wellbore wall and along the crack face. Also, hoop stress distribution is observed by changing the model parameters and the smearing effect idea is discussed.

4.1.1. Hoop Stress Analysis at the Wellbore for Different Stress Anisotropy

Hoop stress analysis is an important way to investigate the stresses at the wellbore wall. Figure 34 shows the hoop stress distribution at the wellbore wall; without a crack at the wellbore wall; with a 6 inch crack at the wellbore wall; and with sealing at the fracture mouth. The horizontal stresses are equal in this figure as $S_{min}=S_{max}$. The sealing materials exist at the fracture mouth that is located an inch inside the six inch fracture. According to Figure 34, the smearing effect is achieved close to the fracture mouth. Between 5^o and 40^o the hoop stress increases dramatically, almost 3000 psi. After 40 degrees the hoop stress decreases below the opened crack hoop stress distribution. All positive values of hoop stress are compression at the wellbore wall and negative values are tension at the wellbore wall.

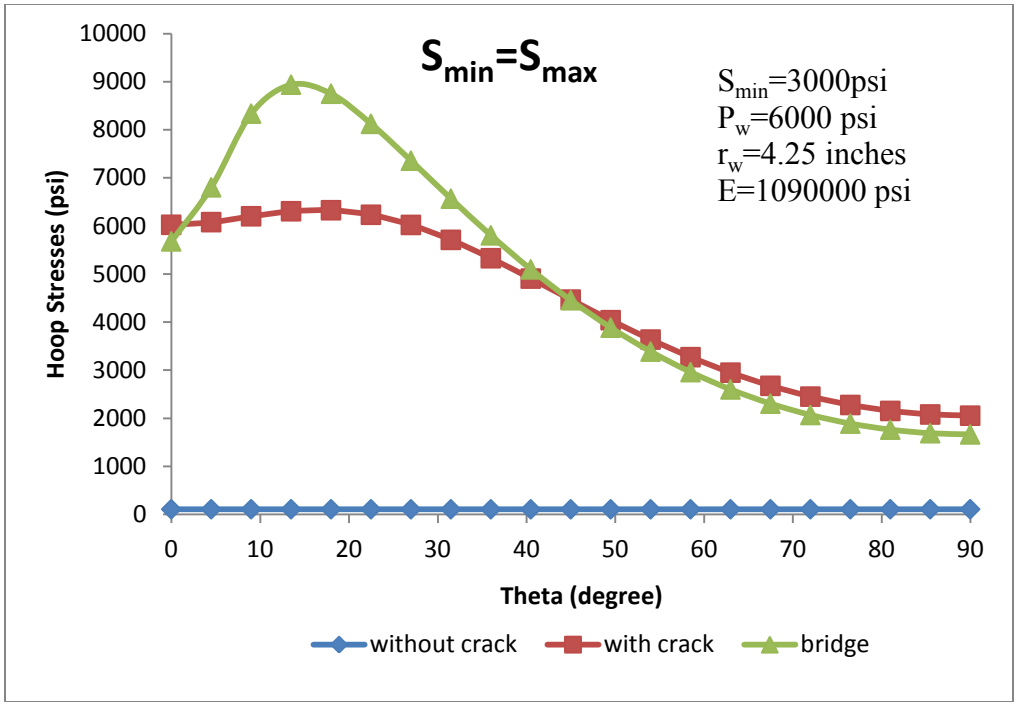

Figure 34. Hoop stress distribution at the wellbore in equal horizontal stresses $S_{min}=S_{max}$

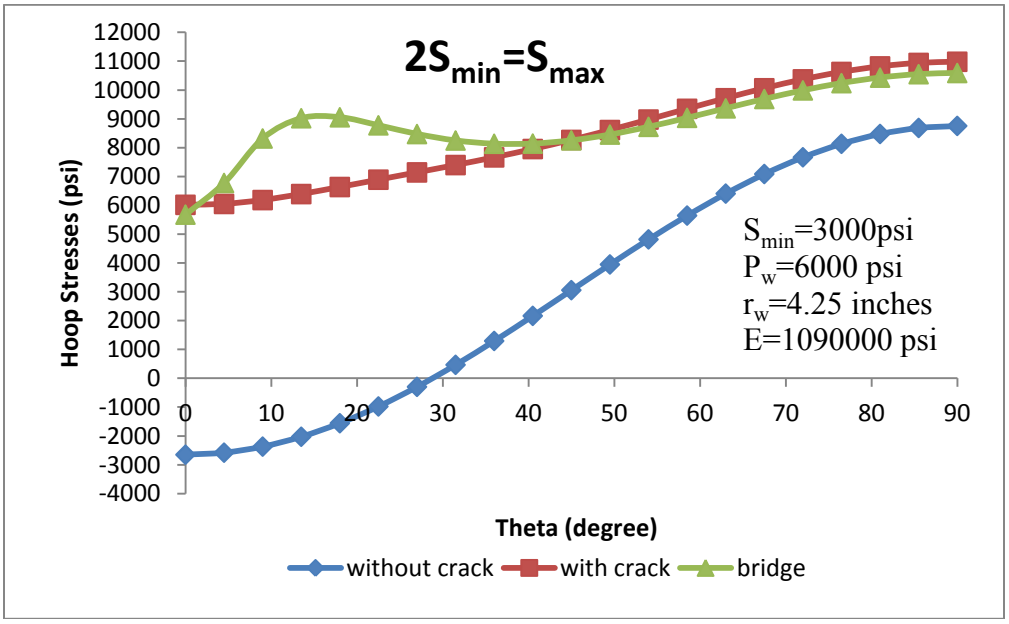

Figure 35. Hoop stress distribution at the wellbore at $2S_{min}=S_{max}$

Figure 35 shows the hoop stress distribution at the wellbore wall when the maximum horizontal stress is twice the minimum horizontal stress. When there is no crack, the hoop stress distribution starts in tension and turns into compression when theta is close to 30 degrees. On the other hand, when there is a crack at the wellbore wall, the hoop stress at the wall starts in compression and increases with increasing theta. Smearing effect is also seen in Figure 35 between degrees of 5^{o}-35^{o}. After 35 degree, it decreases below the hoop stresses of a crack.

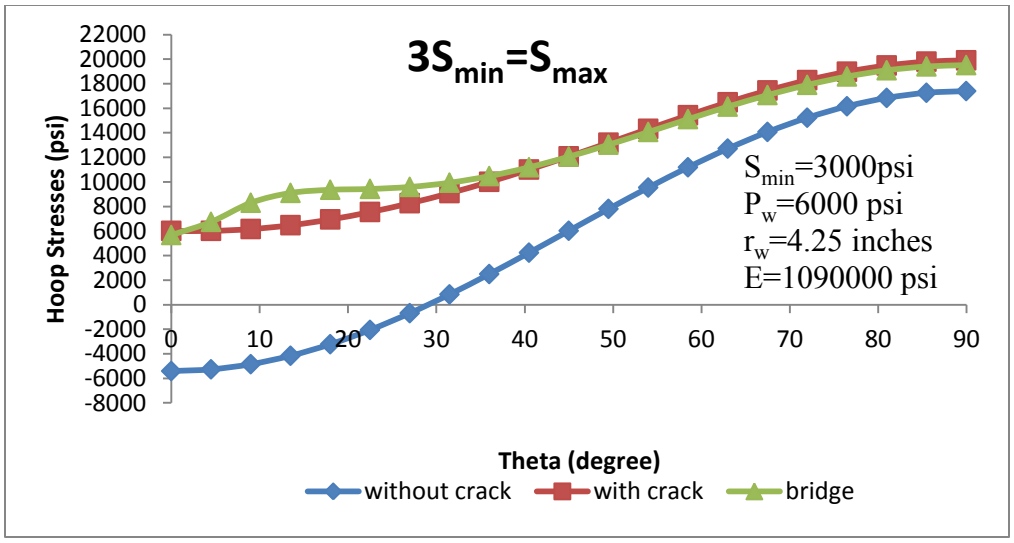

Figure 36. Hoop stress distribution at the wellbore at $3S_{min}=S_{max}$

Figure 36 shows the hoop stress distribution when maximum horizontal stress is three times the minimum one. The smearing effect also is seen and hoop stress along the wellbore wall increases significantly as theta increases.

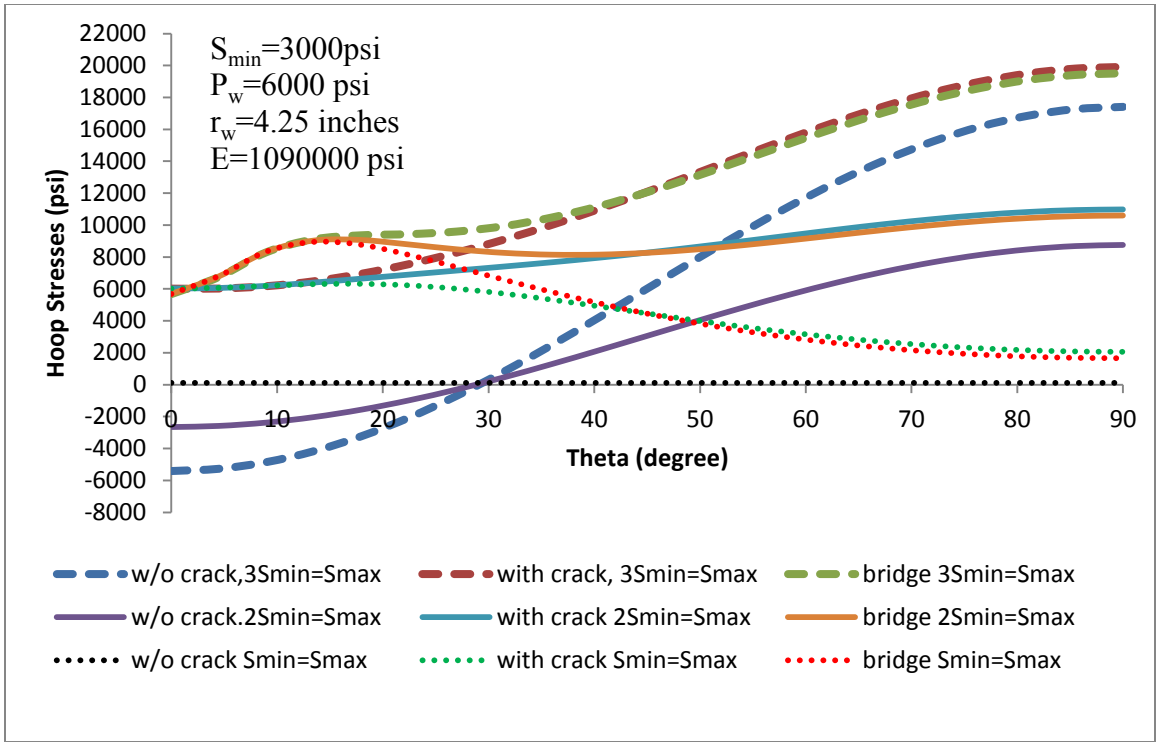

Figure 37. Comparison of hoop stress distribution at the wellbore at different stress anisotropy

In Figure 37, different horizontal stress anisotropies are compared in different scenarios: without a crack at the wellbore wall; with a 6 inch crack at the wellbore wall; and sealing effect (smearing) at the wellbore wall. In three different stress anisotropies, the hoop stress increases at the wellbore wall when bridging materials are applied at the fracture mouth. Bridging materials all increase the hoop stress close to the fracture and between the degrees of 0^o to 25^o the increases are instant. After 25^o, the increase in hoop stress at the wellbore is dramatic only when the maximum horizontal stress is three times the minimum horizontal stress. From Figure 37, when the stress anisotropy is high between the horizontal stresses under the same situations, smearing effect is achieved effectively and hoop stress increase is significant along the wellbore wall.

4.1.2. Hoop Stress Analysis along the Fracture

Hoop stress along the crack face is shown in Figure 38, where the maximum horizontal stress is twice the minimum horizontal stress. The wellbore pressure is 6000 psi and pressure inside the fracture is the same as the wellbore pressure shown in the figure, when there is no crack at the wellbore surface, the hoop stress starts in tension and turns into compression at 1 inch into the fracture trajectory. When there is a 6 inch crack at the wellbore, the pressure inside the crack is 6000 psi and it is all compression. When there is a bridge close to the crack mouth 1 inch distance from the mouth, there is an increase in hoop stress at the bridge location and then it starts to decrease as crack length increases.

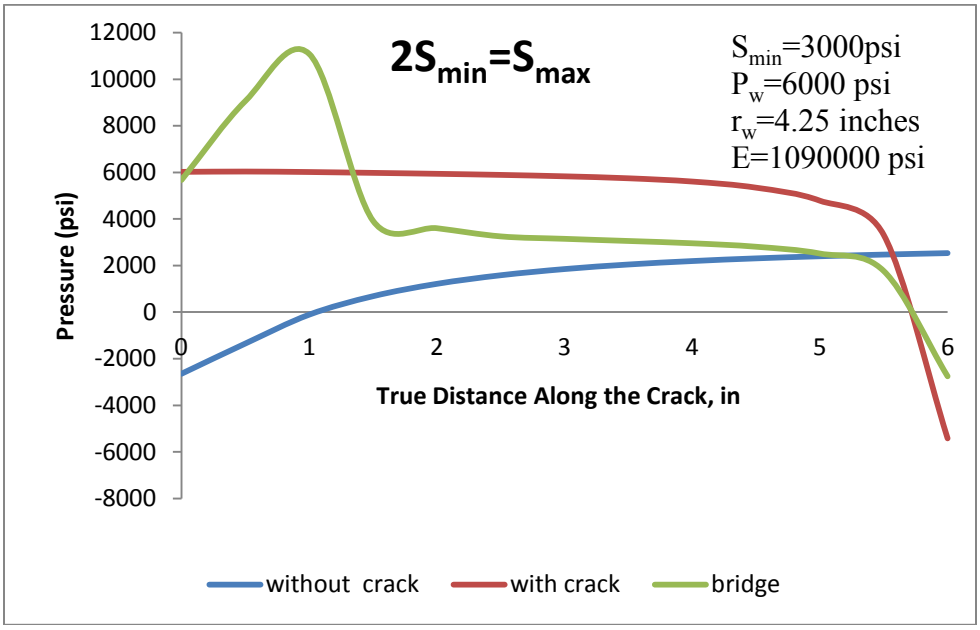

Figure 38. Hoop stress distribution along the crack length

4.1.3. Hoop Stress Analysis at the Wellbore for Different Wellbore Pressures

For different wellbore pressures, the hoop stresses at the wellbore wall change but trend is the same. Figure 39 shows the hoop stresses distribution at the wellbore for 6000 psi wellbore pressure and 7000 psi wellbore pressure. When wellbore pressure is 7000 psi, the hoop stress at the bridge location is higher than 6000 psi wellbore pressure. On the other hand, after sealing, hoop stress is almost the same with the 6000 psi wellbore pressure trend.

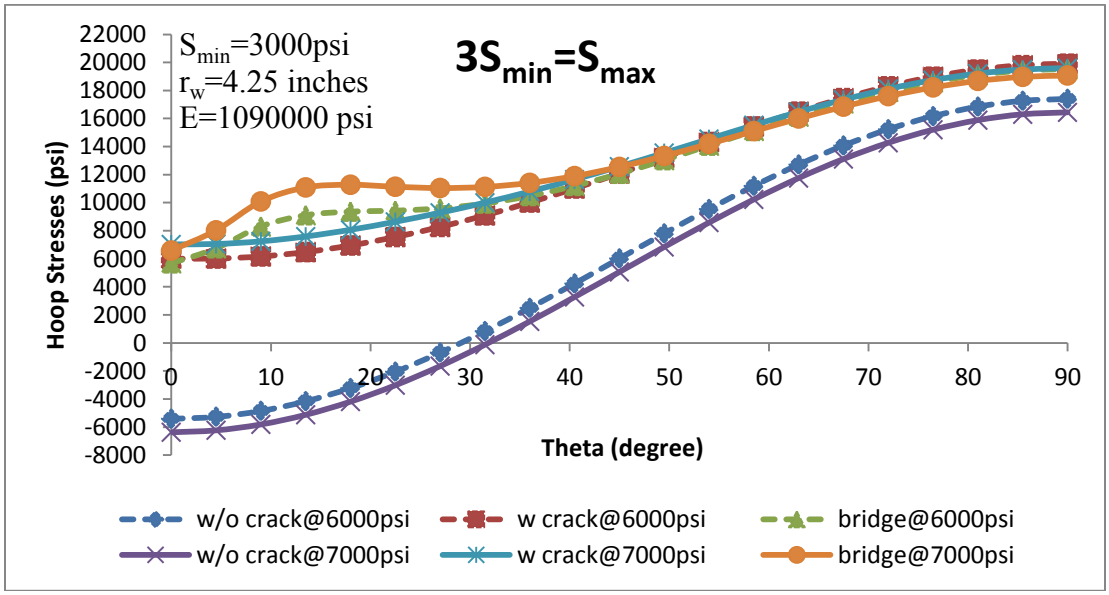

Figure 39. Hoop stress distribution for different wellbore pressures

4.1.4. Hoop Stress Analysis at the Wellbore for Different Young Modulus

Young modulus has no affect for hoop stress analysis at the wellbore wall, shown in Figure 40 for young modulus E_1=1090000 psi and E_2=2000000 psi. In Figure 40, hoop stress distribution at the wellbore wall is the same for two different Young modulii.

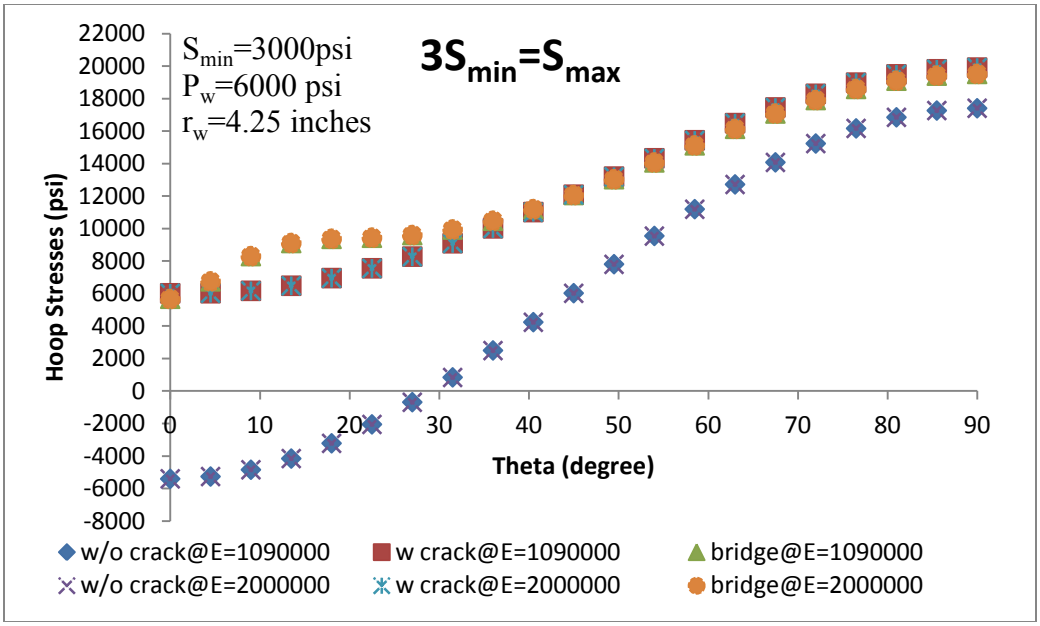

Figure 40. Hoop stress distribution for different Young Modulus

4.1.5. Hoop Stress Analysis at the Wellbore for Different Sealing Locations

Sealing location or bridging location has an important role in the smearing effect of casing drilling. From Figure 41, when the sealing location is close to the crack mouth, it increases the hoop stress at the wellbore wall more than further locations. In Figure 41, sealing locations are 0.5 inch; 1 inch; 2 inches; and 3 inches from the fracture mouth. The closest seal 0.5 inch is the best in increasing the hoop stresses between the angles of 0-35 degree. After 35^o the hoop stress increase is the same for all bridging locations. As the bridging location gets further from the fracture mouth, the hoop stress change is less. For 2 inches and 3 inches, the effect of the sealing location gives the same increase in hoop stress at the wellbore wall.

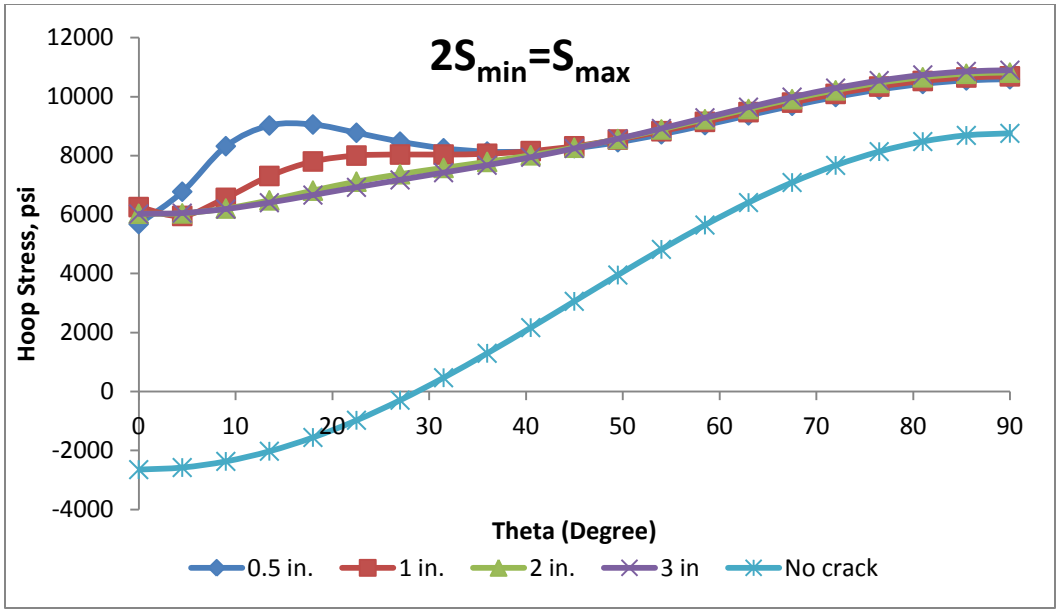

Figure 41. Hoop stress distribution for different sealing locations

4.1.6. Fracture Half-Width for Different Far Field Stress Anisotropy

For different stress anisotropies, the fracture half width changes differently. When stress anisotropy is higher, the fracture width is greater so more stress anisotropy causes more fracture width opening at the wellbore wall. In Figure 42, the fracture widths for different stress anisotropies and closed fracture widths are seen for different in situ stress fields. For horizontal stresses equal, the fracture width is smaller, and it is much easier to narrow down the fracture width by applying sealing at the wellbore wall. When in situ stress differences are high, the fracture width is big and narrowing down the fracture width does not provide perfect sealing to increase the hoop stresses around the wellbore. From Figure 42, narrow and tiny fractures provide better sealing.

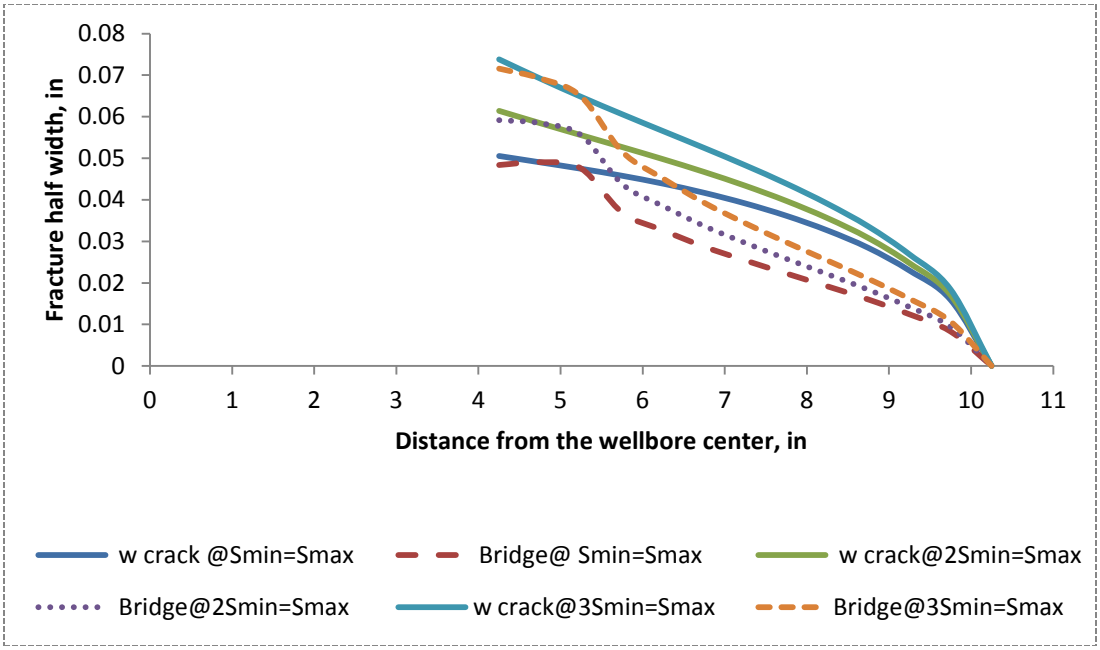

Figure 42. Fracture half width for different stress anisotropy

4.2. Results and Discussion with Initial Porous Fluid In the Model

In this part, a model is generated with initially porous fluid and stress analysis is done at the wellbore wall and along the crack face. Also, the hoop stress distribution is compared with model results that have no porous fluid. In the model, initial pore pressure is 3000 psi and it is equal everywhere in the model.

4.2.1. Hoop Stress Analysis for Different Stress Isotropy at the Wellbore

For different stress anisotropies, the hoop stress distribution at the wellbore wall is shown in Figure 43, 44 and 45. All the hoop stress distribution trends except for equal in situ stresses are the same as with the without pore pressure models that are discussed in the previous section. In Figure 43, when there is no crack, there is all tension at the wellbore wall. When there is a crack it starts into compression and turns into tension after 60 degrees. When there is a bridge at the fracture mouth, the bridge causes increased hoop stress between 0^{o}-40^{o}. Then, hoop stress becomes tensile after 55^{o}.

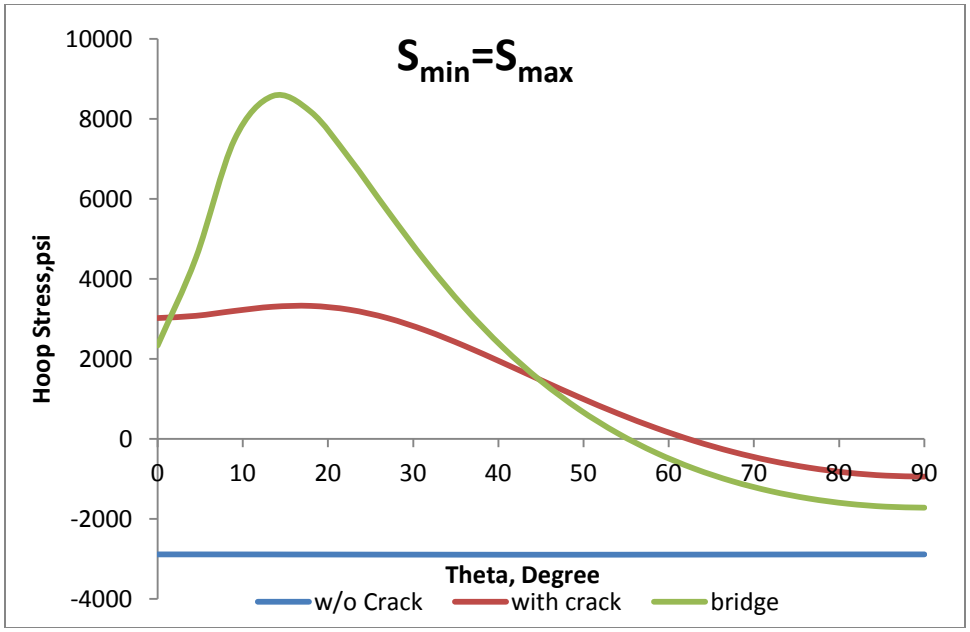

Figure 43. Hoop stress distribution at the wellbore in equal horizontal stresses $S_{min}=S_{max}$ with pore fluid pressure

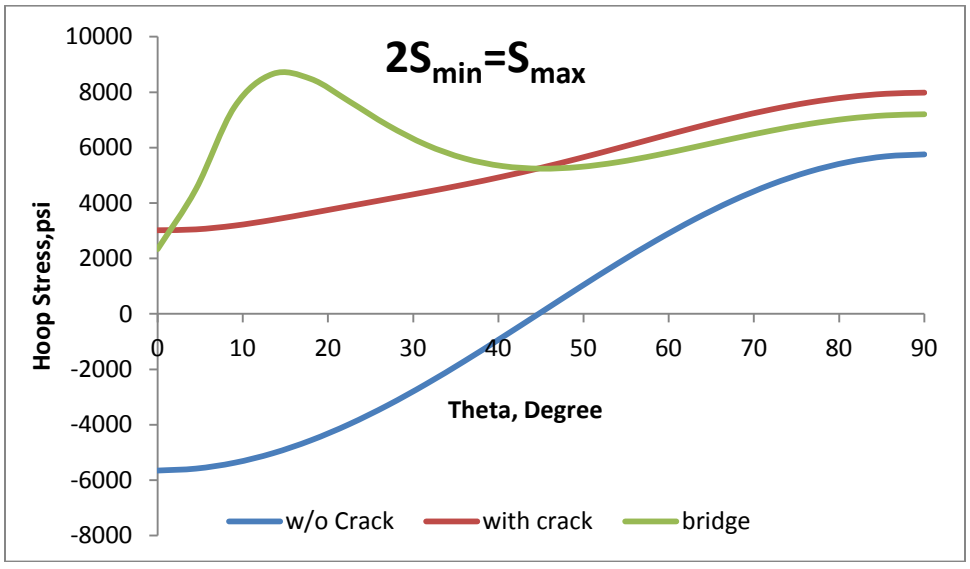

Figure 44. Hoop stress distribution at the wellbore in $2S_{min}=S_{max}$ with pore fluid pressure

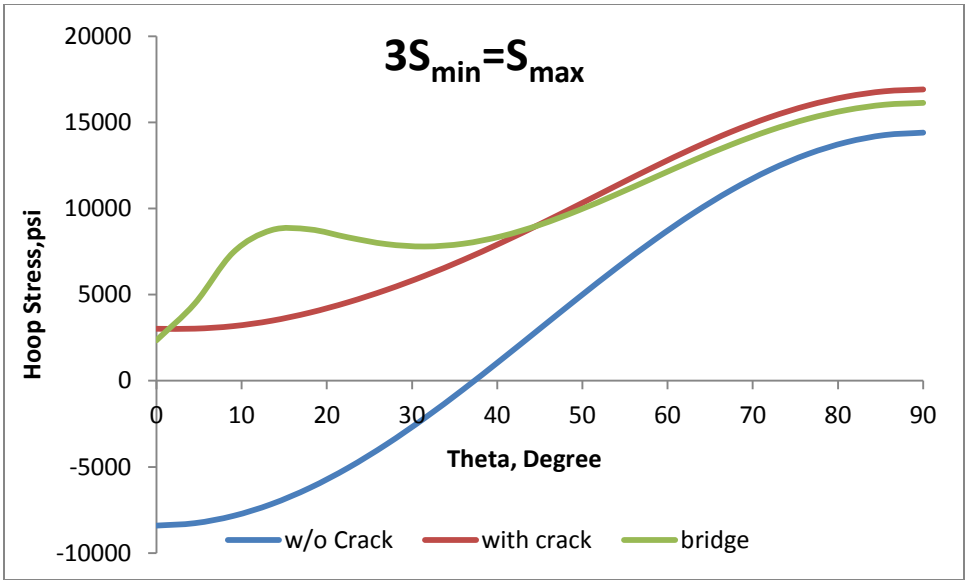

Figure 45. Hoop stress distribution at the wellbore in $3S_{min}=S_{max}$ with pore fluid pressure

As shown in the Figure 44 and 45, when there is no crack, the hoop stress starts as tension at 0^o and turns into compression. When there is a 6 inch crack at the wellbore, the hoop stress starts at 3000 psi as compression and increases proportionally with increasing theta. When bridging is achieved, the hoop stress makes a large increase at the wellbore between 0 and 30 degrees, then increases after this jump.

4.2.2. Comparison Tangential Stress at the Wellbore Wall between With and Without Porous Fluid in Model

Comparisons with and without porous fluid are useful to understand porous fluid behavior and effects in hoop stress distribution at the wellbore wall. From Figure 46, when there is an initial pore fluid, the hoop stress decreases by the amount of initial pore pressure. In this Figure, the initial pore pressure is 3000 psi everywhere.

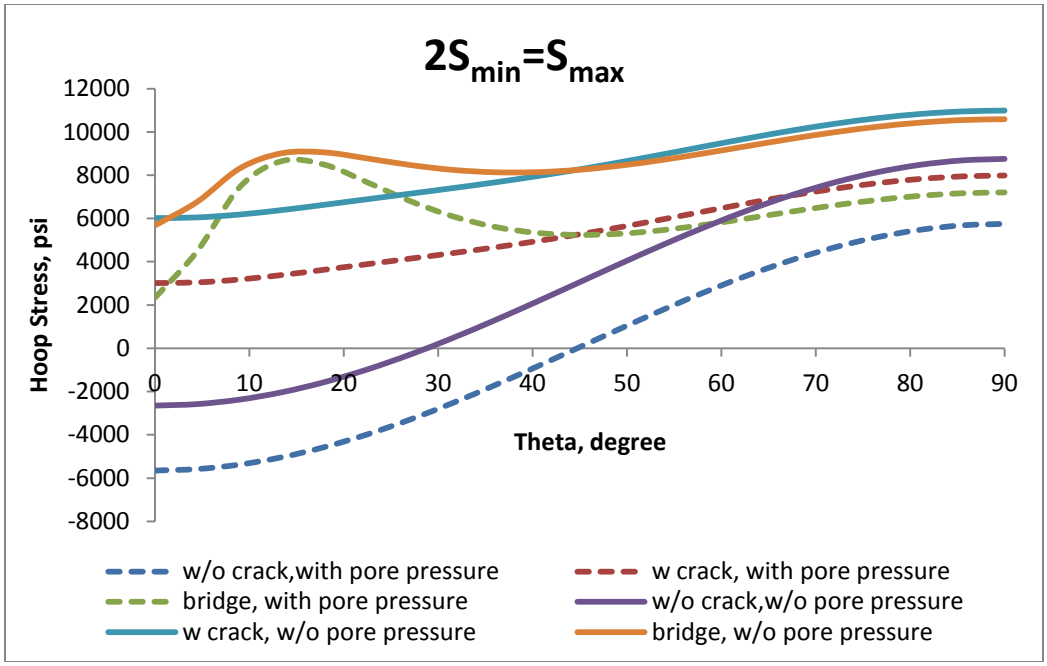

Figure 46. Comparison hoop stress distribution between with pore fluid model and no pore fluid model at the wellbore

In Figure 46, the maximum horizontal stress is twice the minimum horizontal stress and minimum horizontal stress is 3000 psi. When there is no crack at the wellbore wall, the hoop stress distribution is 3000 psi less with the pore fluid model which corresponds to no pore fluid. It is also same when there is a crack at the wellbore wall. The trend of the hoop stress distribution is the same for both models with or without pore fluid. With pore fluid, the tangential stress distribution is 3000 psi less than the no pore fluid model. On the other hand, there is a sharp increase with smearing effect with porous fluid model compared to the non porous fluid model between 0^o and 30^o. After 30^o, the tangential stress decreases below the tangential stress of existing crack and it is also less than for a no pore fluid model.

4.2.3. Comparison Tangential Stress along the Fracture between With and Without Porous Fluid inside Model

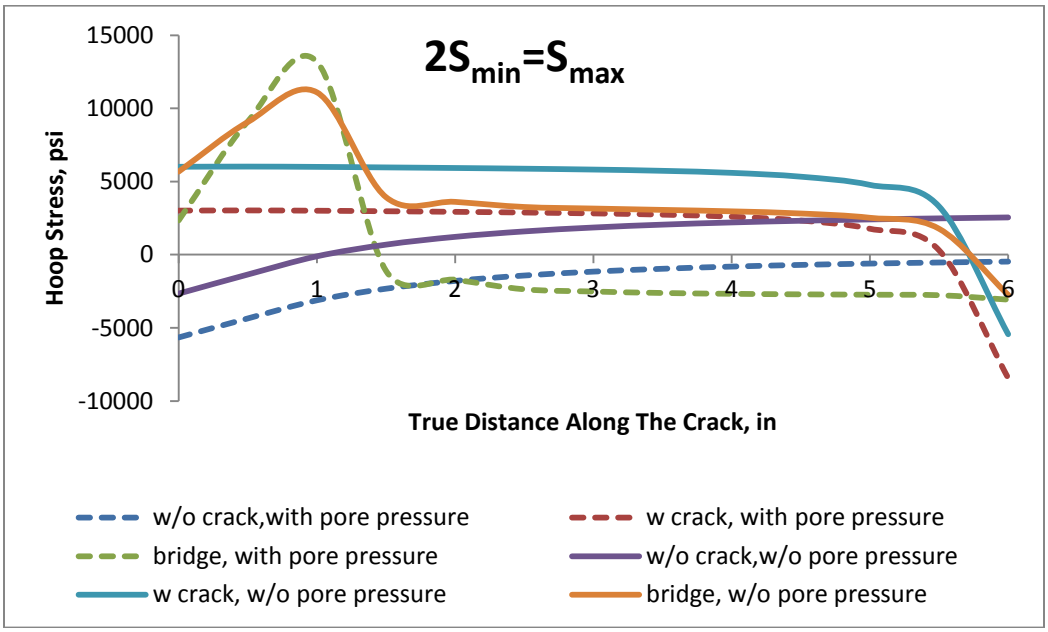

Figure 47. Comparison hoop stress distribution between with pore fluid model and no pore fluid model along the fracture

Figure 47 shows a comparison of tangential stress along the crack face, with and without pore fluid. The trend and the difference is the same between hoop stresses when there is no crack and there is a crack at the wellbore wall. On the other hand, with smearing, the hoop stress increase is larger with pore pressure than without pore pressure in the simulation. There is a significant increase at the fracture mouth where bridging is achieved when there is a pore pressure. Beyond the bridging location, the hoop stress along the crack face becomes tensile and it is nearly constant along the fracture face.

4.2.4. Comparison Tangential Stress at the Wellbore Wall between With and Without Porous Fluid inside Model for Different Sealing Locations

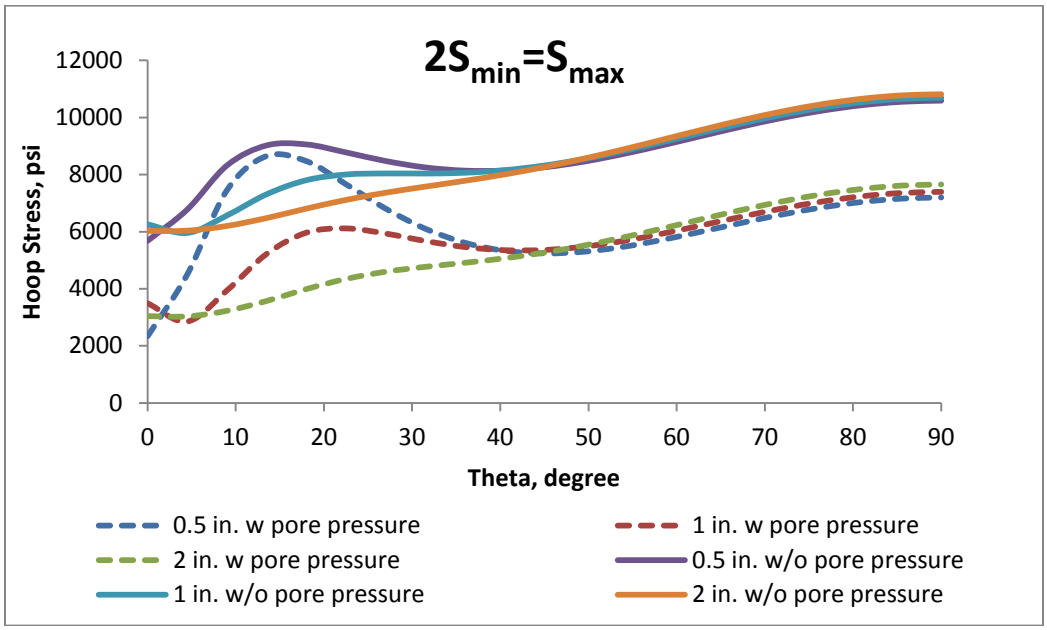

Figure 48. Comparison hoop stress distribution between with pore fluid model and no pore fluid model at the wellbore for different sealing locations

Figure 48 summarizes hoop stress distribution for different sealing locations with pore pressure and without pore pressure where $2S_{min}=S_{max}$ and minimum in situ stress is 3000 psi. It can be seen that tangential stress has increased along the wellbore, with more increases close to the fracture mouth. Closer to the fracture mouth, smearing effect is more efficient as the bridge gets closer to the fracture tip, the hoop stress along the wellbore also increase but at a lower rate. Hoop stress increases along the wellbore for the model that has no pore pressure. All in all, the best location for bridging is close to a fracture mouth that has pore pressure.

4.2.5. Comparison Fracture Half-Width between With and Without Porous Fluid in Model

Figure 49 demonstrates a fracture half width comparison between the model with pore pressure and without pore pressure when $2S_{min}=S_{max}$. Sealing is perfectly achieved when there is pore pressure and fracture closure is much more efficient than without pore pressure. In both models, the fracture shapes are the same for the initial conditions. After applying bridging, the closure along the fracture is higher in the model with pore pressure than without pore pressure. Pore pressure helps close the fracture when smearing particles are applied close to the fracture mouth. In conclusion, when there is pore pressure, fracture closure is achieved and thus, hoop stresses along the wellbore increase efficiently by the smearing effect.

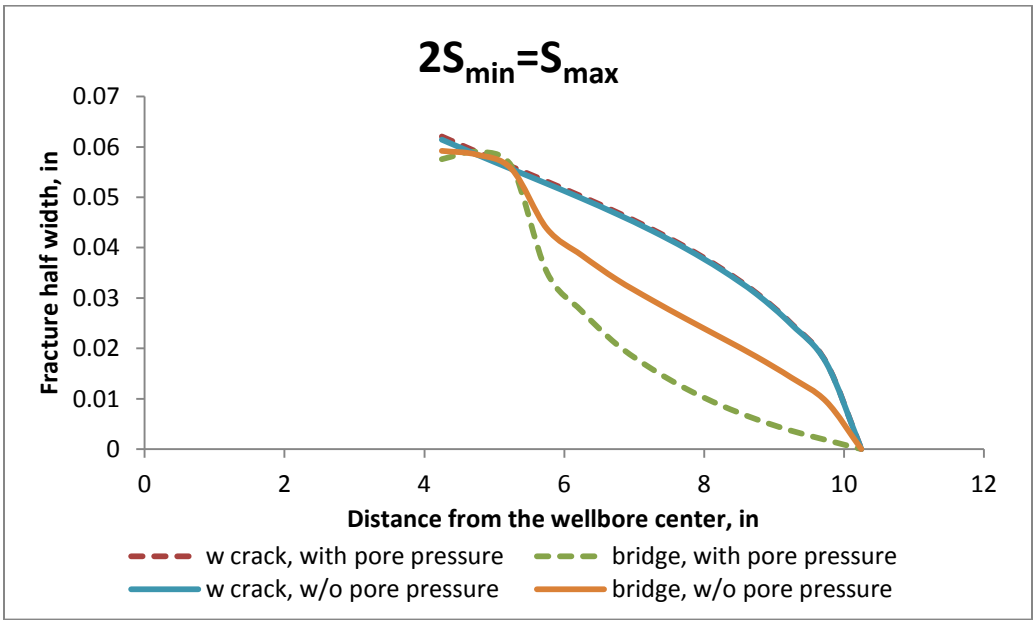

Figure 49. Comparison fracture half-width between with pore fluid model and no pore fluid model

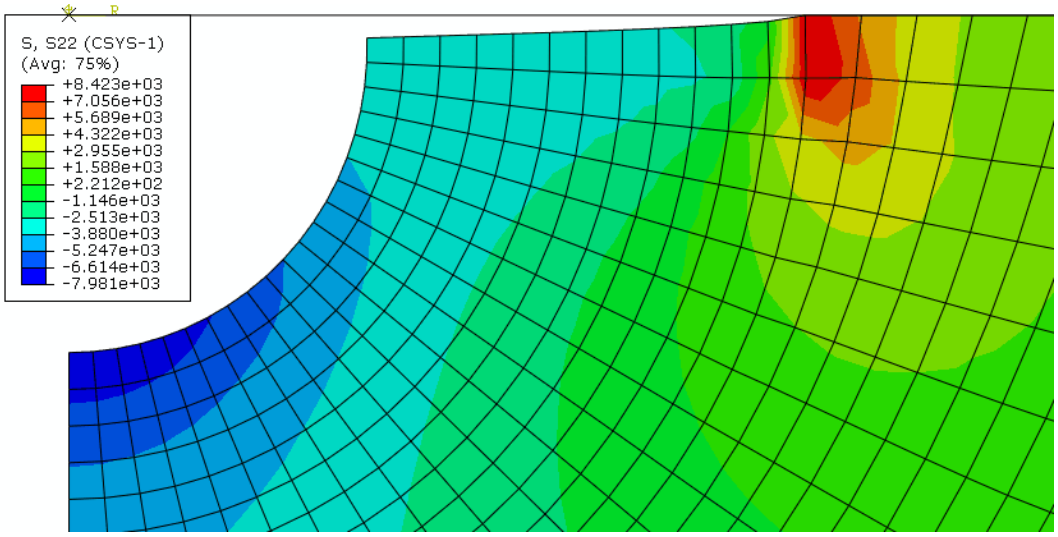

Figure 50. Fracture half-width in pore fluid model

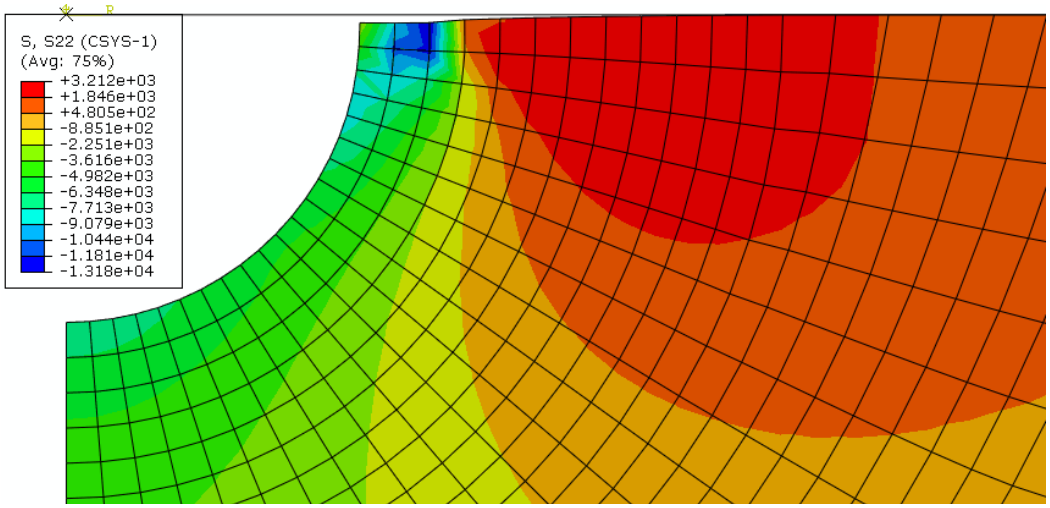

Figure 51. Fracture closure in pore fluid model after applying sealing

In Figures 50 and 51, the fracture half width and fracture closure are shown after applying an initial pore pressure in the model. The positive values of the stresses are tension in ABAQUS and negatives are compression. At the fracture tip in Figure 50, there is a tension and stress concentration is high at the fracture tip. According to Figure

51, when applying a bridge close to the fracture mouth, at the bridge location there is a compression and after the bridge, it turns into tension. All the hoop stresses around the wellbore and along the fracture are seen in Figure 50 and 51.

4.3. Results and Discussion with Porous Fluid Flow In the Model

In this part of the study, the model is generated with saturated porous fluid flow. First, the pore fluid flow velocity is defined as 0.7 in/min and all hoop stress distributions are calculated and pore pressure distribution is generated. Then, a 3 in/min pore fluid velocity is applied and all the stress analysis are done and compared to the 0.7 in/min model. Pore fluid flow is applied to the wellbore, inside fracture, and before and after the bridge location to simulate fluid leakage into the formation. Geostatic and soil transient steps are used to generate pore fluid flow in the model. Also, results are compared with an initial pore pressure inside and pore fluid flow.

4.3.1. Hoop Stress Analysis for Different Stress Isotropy at the Wellbore

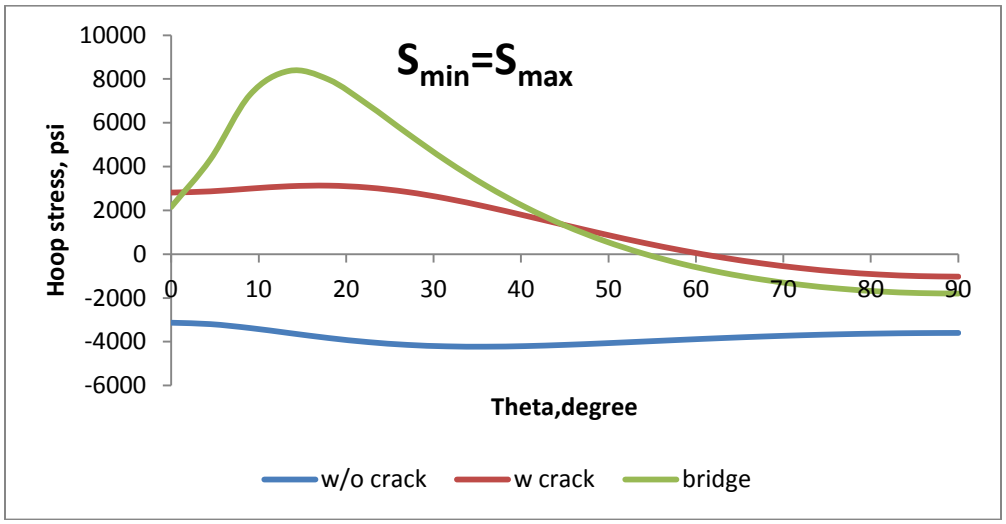

Figure 52. Hoop stress distribution at the wellbore $S_{min}=S_{max}$ with pore fluid flow

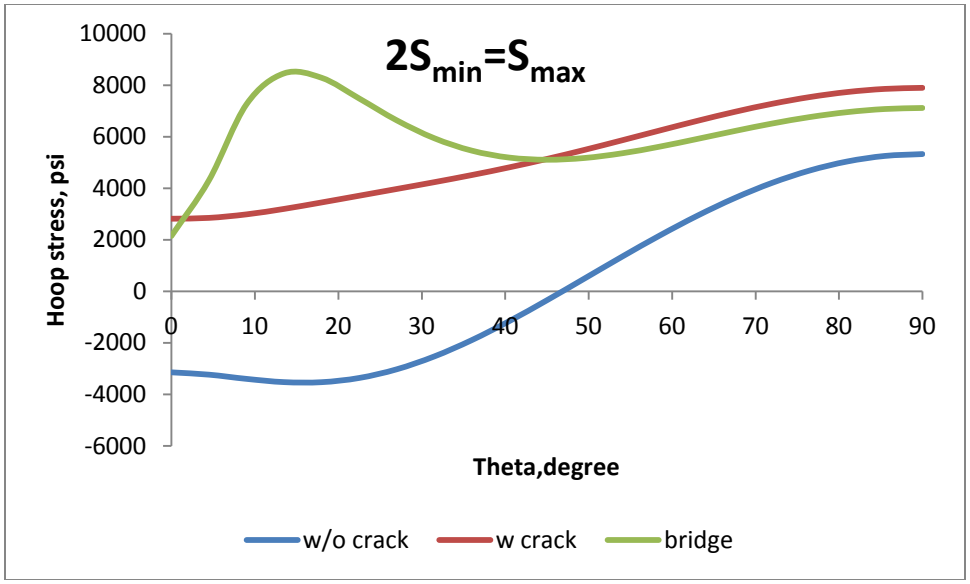

Figure 53. Hoop stress distribution at the wellbore $2S_{min}=S_{max}$ with pore fluid flow

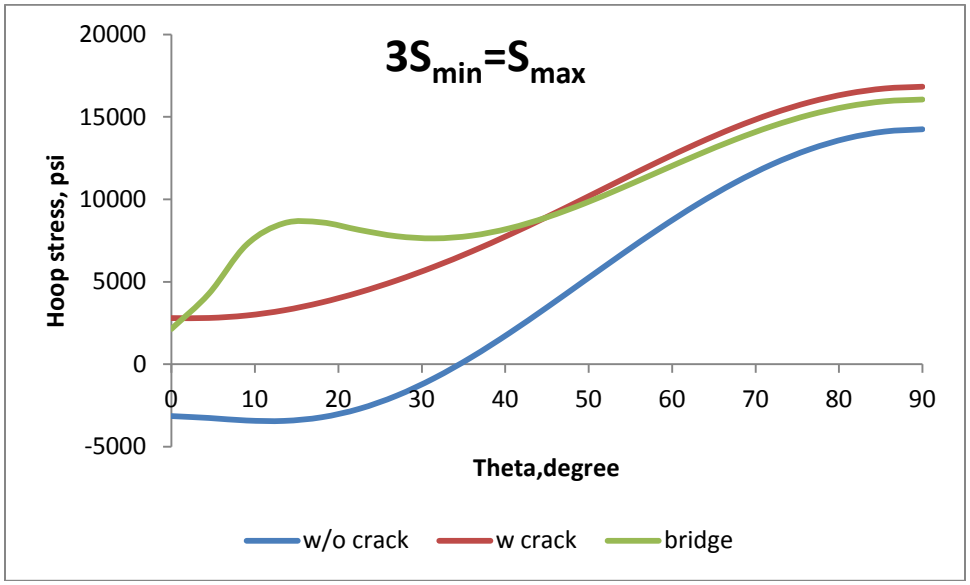

Figure 54. Hoop stress distribution at the wellbore $3S_{min}=S_{max}$ with pore fluid flow

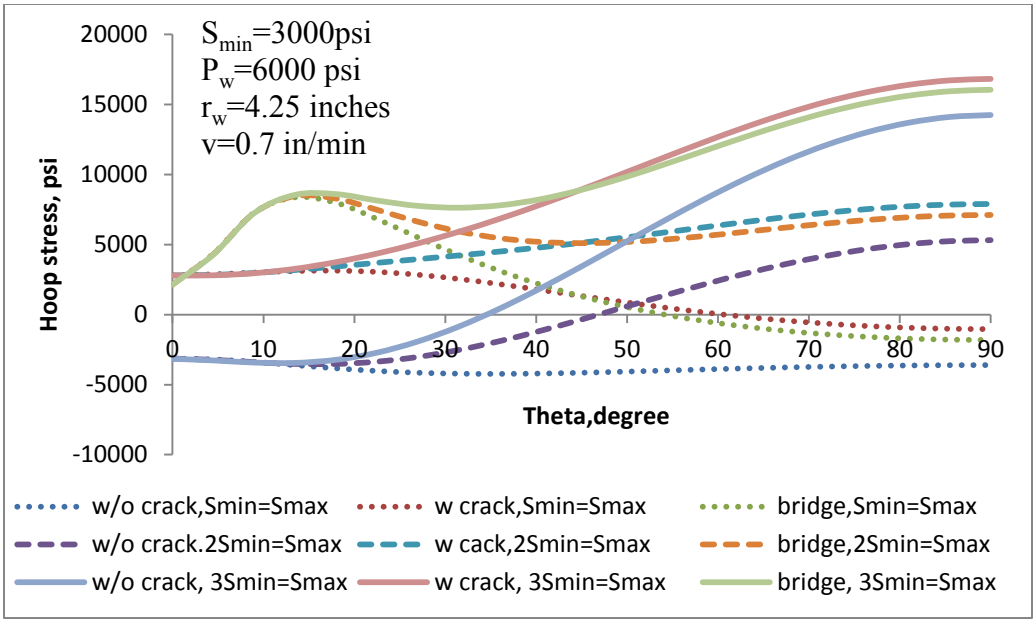

Figure 55. Comparison of hoop stress distribution at the wellbore at different stress anisotropy for pore fluid flow

In Figures 52, 53, and 54, the hoop stress distributions at the wellbore wall are shown for different stress anisotropies: $S_{min}=S_{max}$; $2S_{min}=S_{max}$; $3S_{min}=S_{max}$. In all different stress anisotropies, the smearing effect is achieved between 0-30 degree and only when the stress anisotropy is $3S_{min}=S_{max}$, the hoop stress keeps increasing at the wellbore wall. The pore fluid flow velocity is 0.7 in/min in the entire model.

In Figure 55, all three stress anisotropies are compared for pore fluid flow in the model. It is concluded from the figure that the smearing effect is achieved close to the fracture from 0^o and 30^o. When the in situ stress anisotropy is large, hoop stress increases are high around the wellbore wall.

4.3.2. Hoop Stress Analysis at the Wellbore for Different Sealing Locations

In Figure 56, the effects of different sealing locations are shown. A sealing location close to the fracture mouth gives the most effective increase in hoop stress at the wellbore. Further away, the sealing effect is less important.

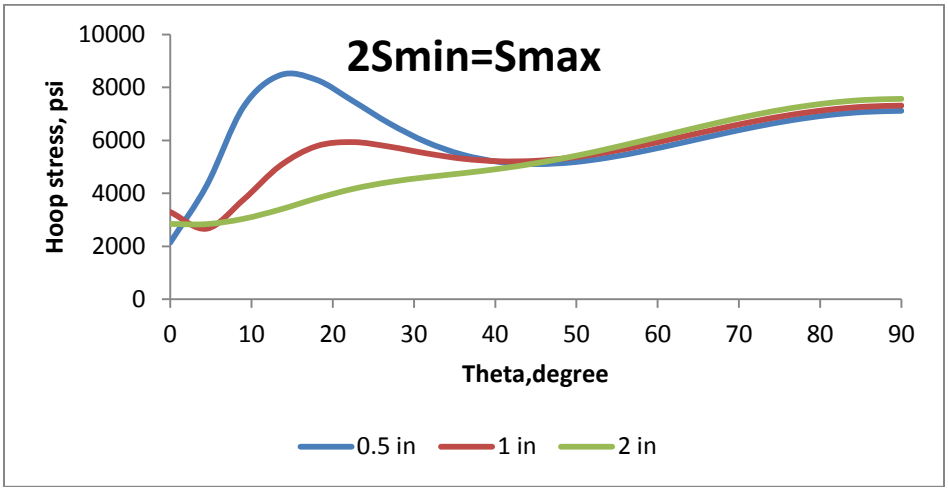

Figure 56. Hoop stress analysis for different sealing location for pore fluid flow

4.3.3. Pore Pressure Distribution at the Wellbore Wall and Along the Model

In Figures 57 and 58, pore pressure distributions at the wellbore and along the model are shown. From Figure 57, pore pressure is constant at the wellbore wall for all values of theta for no crack. Initial pore pressure inside the model is 3000 psi, and when applying pore fluid flow as velocity at the wellbore, it increases the pore pressure at the wall as leaking drilling fluid causes increase in pore pressure. When there is a crack, the pore pressure close to the fracture is high because drilling fluid leaks into the formation. After that, it decreases with theta. Pore pressure distribution along the model width behaves like pore pressure at the wellbore wall. When there is no crack it starts high, and then goes down with increasing distance. When there is a crack, this is the highest pore pressure along the width and when smearing is applied, pore pressure is as high as the

crack pore pressure and goes down by increasing distance from the wellbore. Pore pressure distribution is shown in Figure 59.

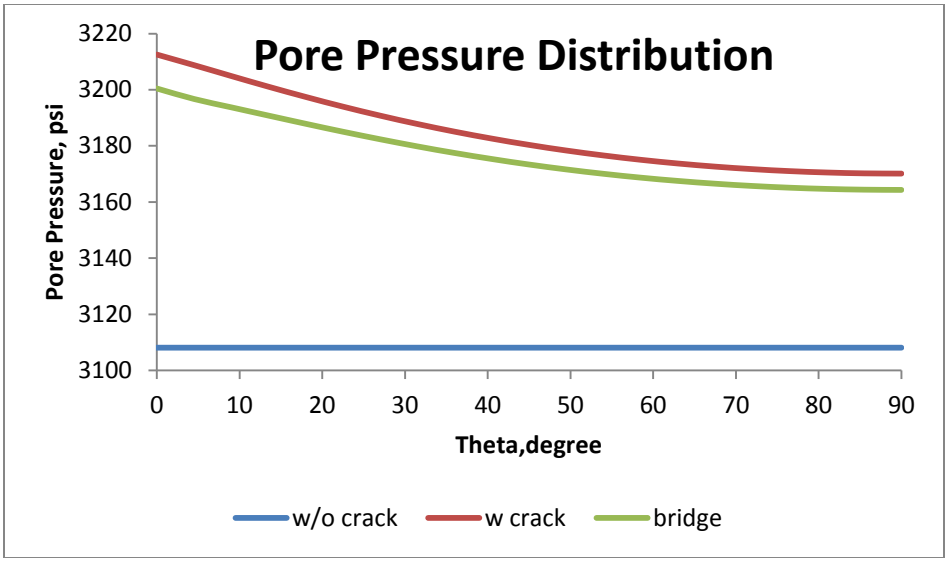

Figure 57. Pore pressure distribution at the wellbore

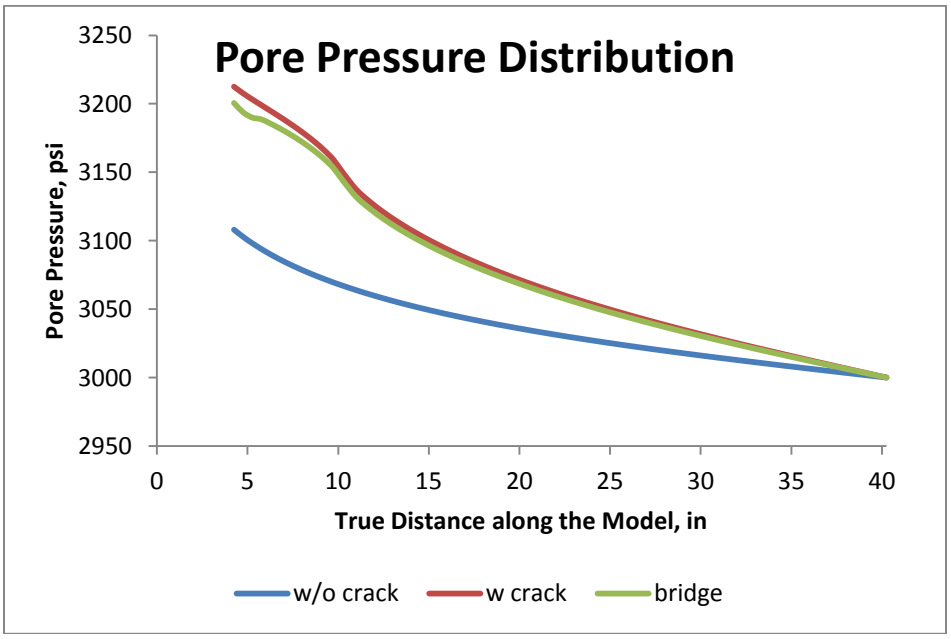

Figure 58. Pore pressure distribution along the model width

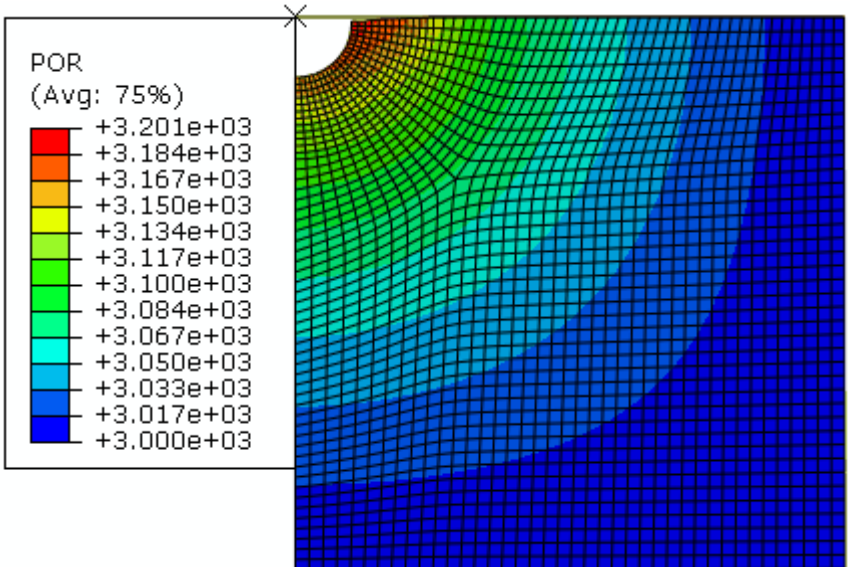

Figure 59. Pore pressure distribution, ABAQUS

4.3.4. Comparison Hoop Stress Analysis with Changing Pore Fluid Flow Velocity at the Wellbore

In Figure 60, hoop stress analysis is done by comparing pore fluid flow velocity at the wellbore wall. Trends in the graphs are the same with changing velocities. When there is no crack, hoop stress starts in tension and turns into compression. When there is a crack, it starts with compression which increases as theta increases. Also, when there is a bridge at the fracture mouth, it increases the hoop stress close to the fracture between 0^o and 30^o.

On the other hand, as pore fluid flow velocity gets higher, the hoop stresses get lower. The faster pore fluid velocity causes lower hoop stress at the wellbore. When pore fluid velocity is high, it leaks into the formation faster and decreases the hoop stress close to the wellbore. The principal total stress is equal to the sum of pore pressure and principal effective stress in the formation. If the pore fluid flow is high, the pore pressure gets high and the effective stress goes down so that the total stress remains the same.

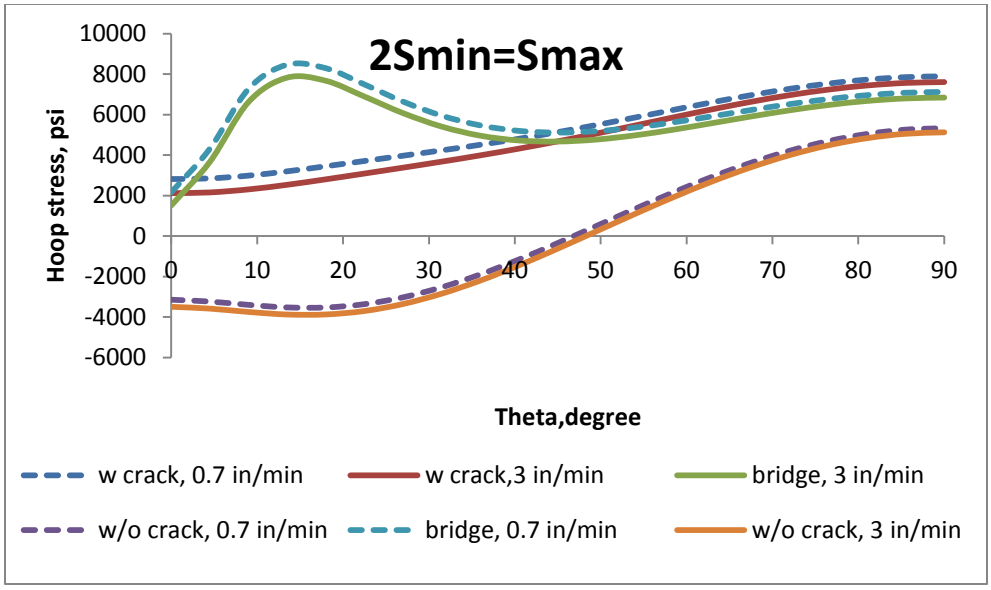

Figure 60. Comparison hoop stress distribution with changing pore fluid flow velocity at the wellbore

4.3.5. Comparison Hoop Stress at the Wellbore with Pore Fluid Flow and Initial Pore Pressure for Different Sealing Locations

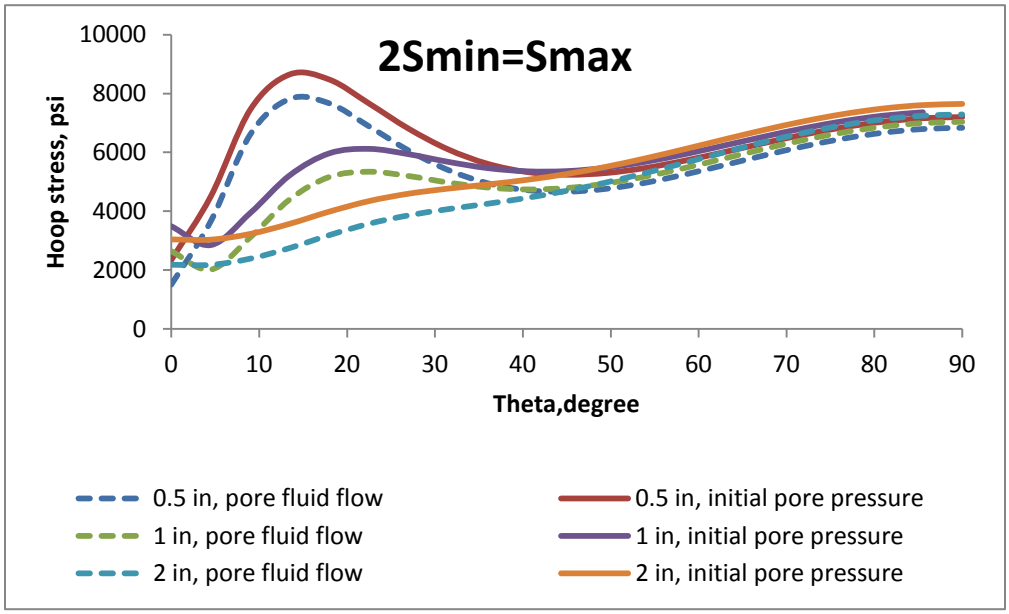

Figure 61. Comparison hoop stress distribution between initial pore pressure model and pore fluid flow model at the wellbore for different sealing locations

Figure 61 shows a comparison of hoop stress at the wellbore between initial pore pressure (3000 psi and does not change), and pore fluid flow inside the model, which has a velocity and leaks from the drilling fluid which changes the pore pressure inside the model. All the hoop stress trends are the same for initial pore pressure and pore fluid flow model, but the pore fluid flow model's hoop stresses are less than the initial pore pressure model at the wellbore. The reason is where pore pressure is high, the effective stresses, which are hoop stresses in the model, go down because the total principal stress should be the same.

4.3.6. Comparison Fracture Half-Width with Changing Pore Fluid Flow Velocity

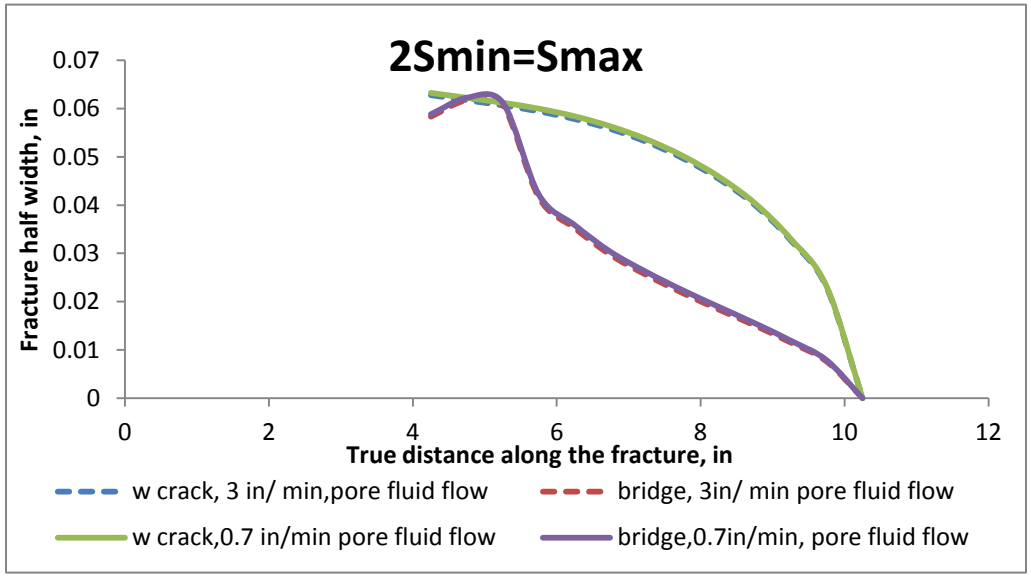

Figure 62. Comparison fracture half width with changing pore fluid flow velocity

Figure 62 shows the fracture half width with changing pore fluid flow velocity in the model. As shown in the figure, there are no changes in the fracture half width and fracture closure width by changing pore fluid flow velocity.

4.3.7. Pore Pressure Distribution along the Model with Pore Fluid Flow Velocity

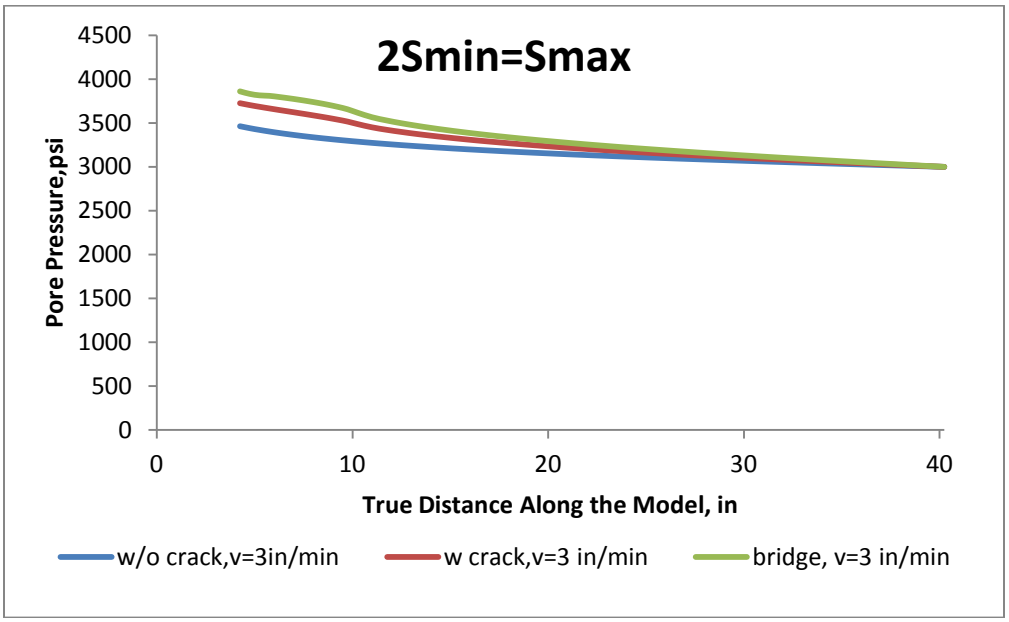

Figure 63. Pore pressure distribution for pore fluid flow velocity is 3 in/min

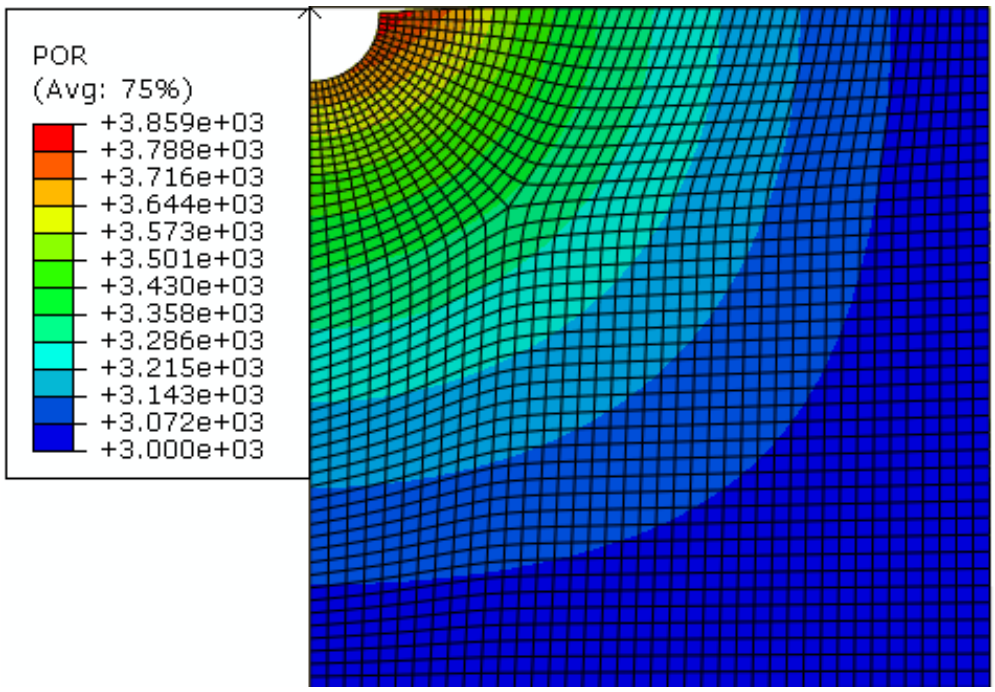

Figure 64. Pore pressure distribution when v=3 in/min, ABAQUS

Figures 63 and 64 show the pore pressure distribution along the model width when 3 in/min pore fluid flow velocity is applied. From Figure 63, when smearing is achieved, pore pressure distribution is higher than the crack and without crack pore pressure distributions. Smearing causes leaking after the bridging location and this increases pore pressure beyond the bridging location. If the formation is permeable enough, leak-off is achieved and drilling fluid behind the smearing location dissipates into the formation which causes an increase in pore pressure before the smearing location. When bridging is achieved, the pore pressure distribution is higher than with the crack and without crack pore pressures.

4.4. Results and Discussion with Multiple Cracks in Extended Finite Element Model (XFEM)

4.4.1. Hoop Stress Distribution for Different Stress Isotropy for Perfect Wellbore Shape

Figure 65 shows multiple cracks in extended finite element model when the wellbore pressure is 7000 psi and horizontal stress isotropy is $2S_{min}=S_{max}$, with minimum horizontal stress of 3000 psi. It can be seen that there are two cracks that are placed close to 90 degree and 270 degree in the wellbore wall. When the wellbore shape is perfectly circular, the cracks open at the same time when the wellbore pressure overcomes the minimum principal stress. The two cracks are symmetric at the wellbore wall when the wellbore shape is perfectly circular. Figure 66 demonstrates the multiple crack hoop stress distribution when the stress state is $3S_{min}=S_{max}$. On the other hand, Figure 67 shows the comparison hoop stress distribution between different stress anisotropies. As concluded from Figure 67, when the stress isotropy is high, the hoop stress increase is high between the two cracks. Thus, wellbore strengthening is achieved effectively when the stress state difference is high in multiple cracks at the wellbore wall.

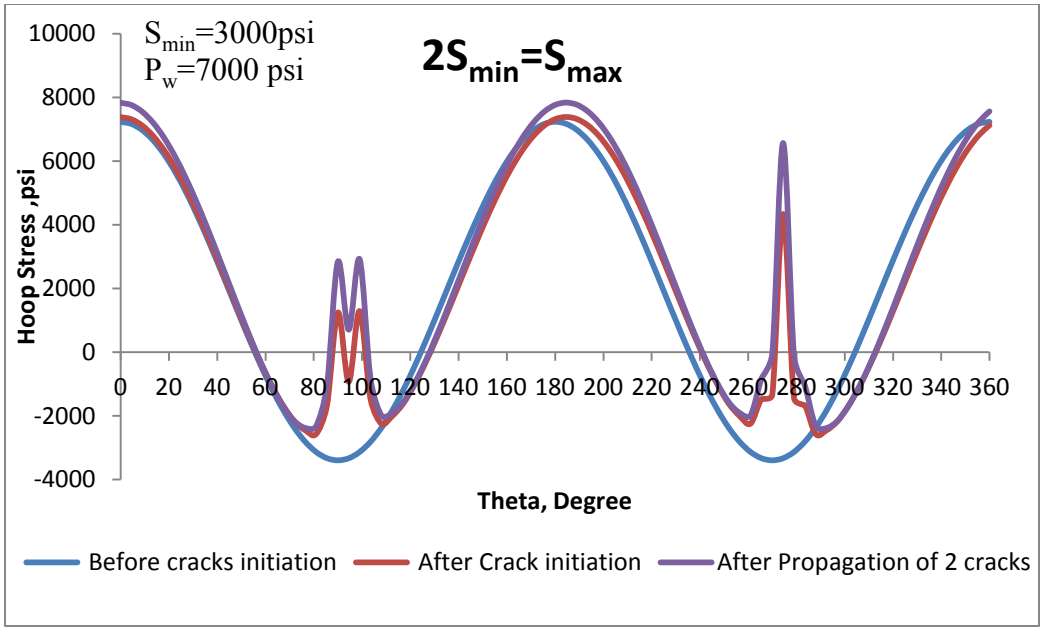

Figure 65. Hoop stress distribution for multiple cracks in perfect wellbore shape, $2S_{min}=S_{max}$

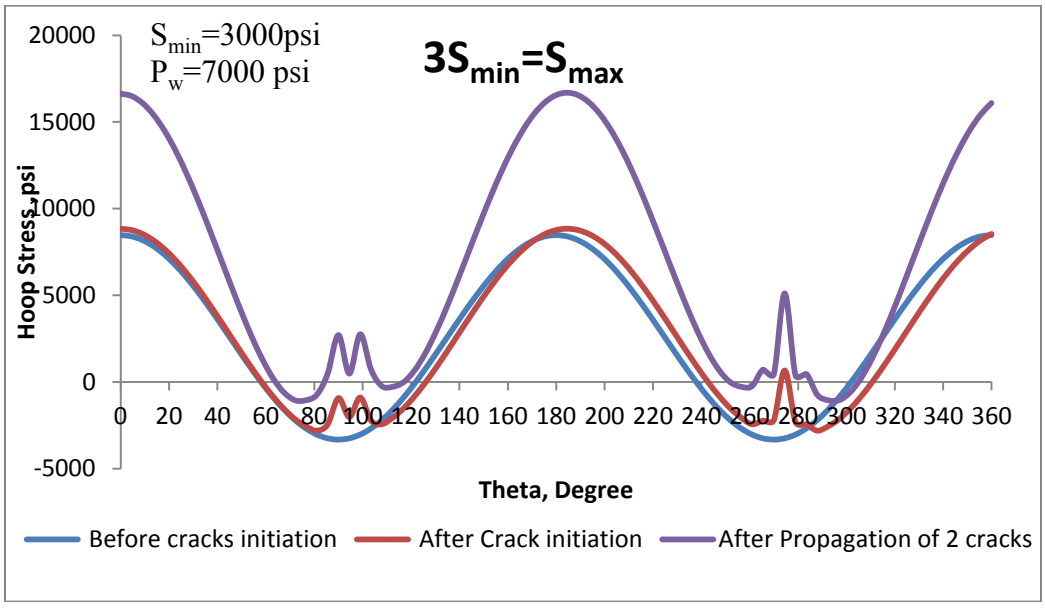

Figure 66. Hoop stress distribution for multiple cracks in perfect wellbore shape, $3S_{min}=S_{max}$

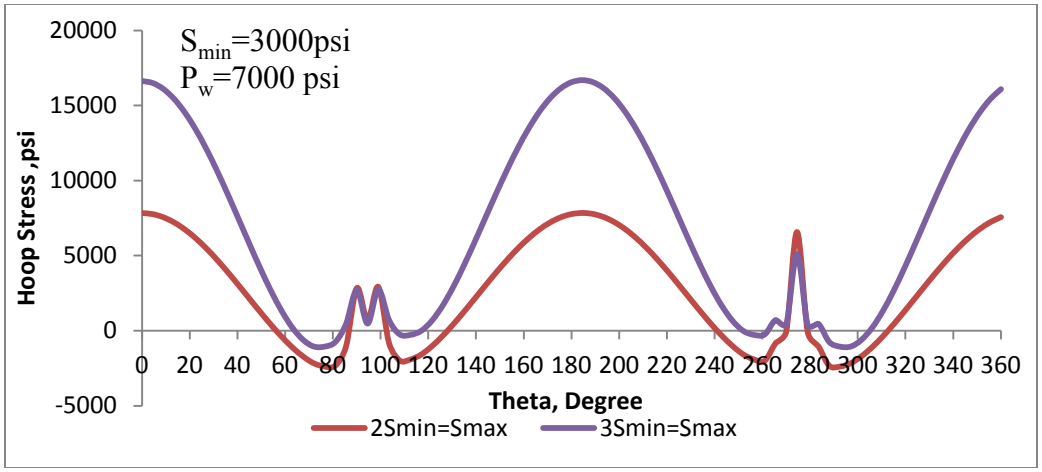

Figure 67. Comparison of hoop stress distribution for different stress state in multiple cracks in perfect wellbore shape

4.4.2. Hoop Stress Distribution for Different Wellbore Pressure for Perfect Wellbore Shape

Figures 68 and 69 show the hoop stress distribution for different wellbore pressures of 7000 psi and 10000 psi in perfect shape wellbores. For the different wellbore pressures, multiple cracks are symmetric and they are perpendicular to the minimum far field stress. The hoop stress is shown just before the crack initiation; after the cracks are initiated; and after the 2 cracks are propagated into the formation. In Figures 68 and 69, the compressive stresses are different at 90^o-100^o than 270^o-280^o because the first crack, which is at 90-100 degree, compresses the adjacent formation by increasing width and increases the second crack hoop stresses at 270^o-280^o. As a result, the second crack's compressive stress is higher compared to first one because of the increasing fracture width in multiple cracks region.

Figure 70 displays the comparison between wellbore pressures of 7000 psi and 10000 psi. When wellbore pressure is different, there is no big effect for crack positions. They are opened at the same position and also the hoop stresses are the same at the crack mouths. On the other hand, when wellbore pressure is low, the hoop stress between two

cracks is higher than the higher wellbore pressure. The compression is high between two cracks and it affects the hoop stress distribution. As a result, the lower wellbore pressure has higher compression hoop stress at the wellbore wall between the two cracks.

Figure 71 shows the hoop stress distribution for multiple cracks in perfect wellbore shape and positive values are tension and negative values are comparison in the legend.

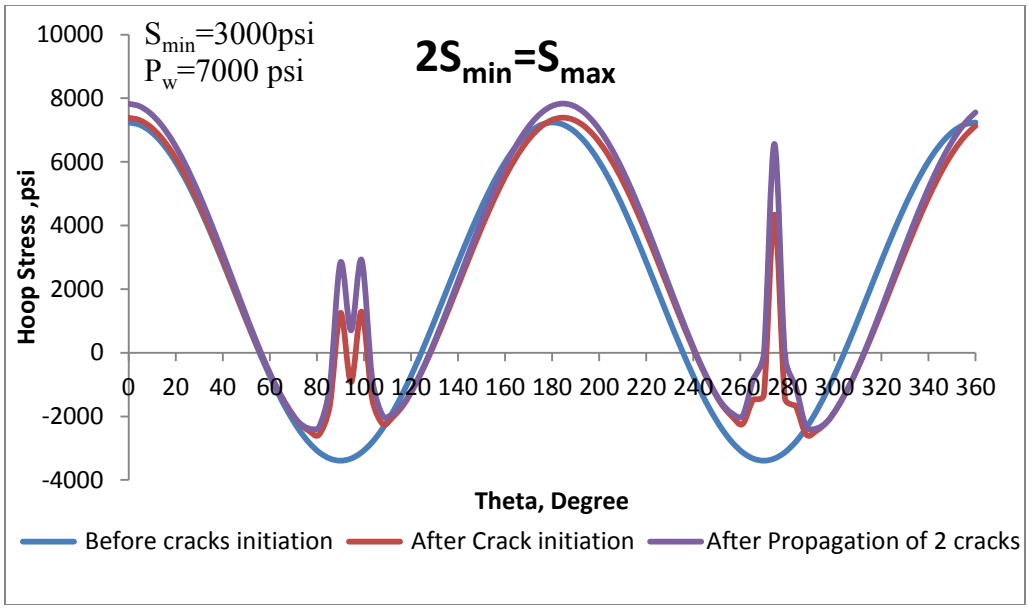

Figure 68. Hoop stress distribution for multiple cracks in perfect wellbore shape, P_w=7000 psi

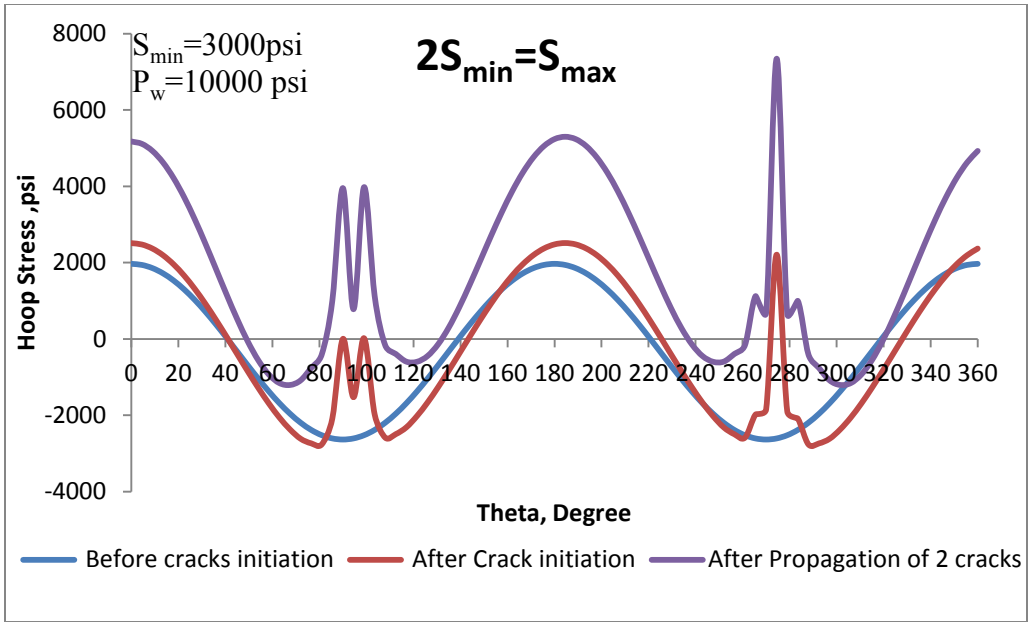

Figure 69. Hoop stress distribution for multiple cracks in perfect wellbore shape, P_w=10000 psi

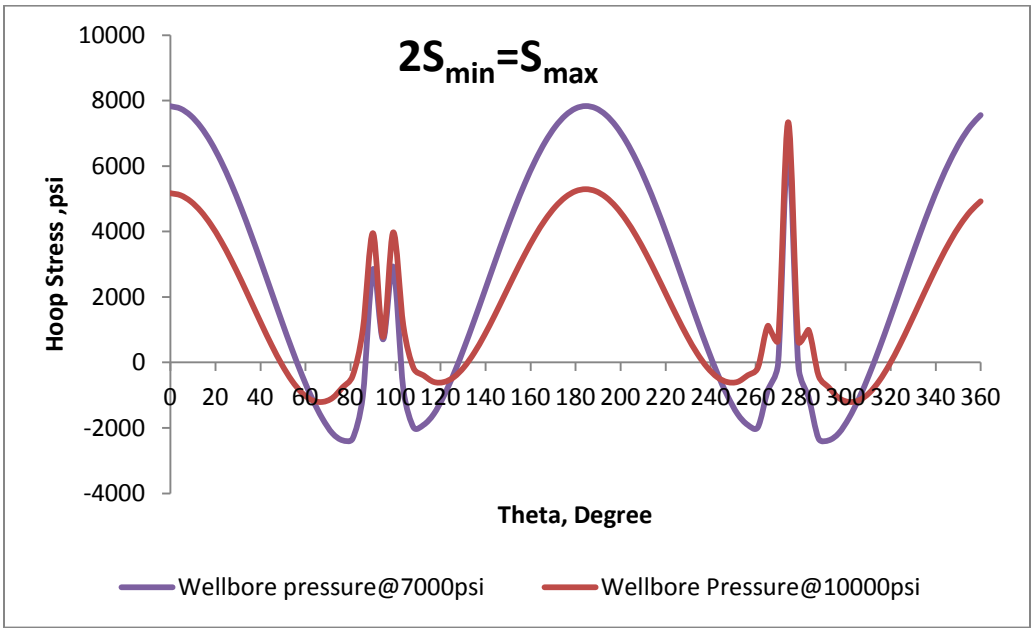

Figure 70. Comparison of hoop stress distribution for different wellbore pressures in perfect wellbore shape

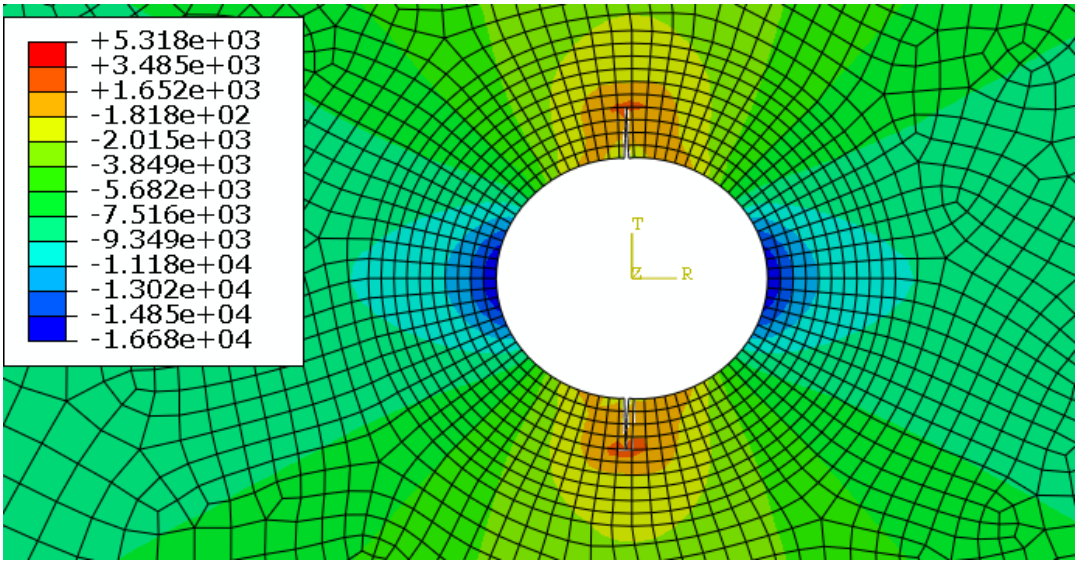

Figure 71. Hoop stress distribution for multiple cracks in perfect wellbore shape, P_w=7000 psi, ABAQUS

4.4.3. Hoop Stress Distribution for Different Wellbore Pressure for Imperfect Wellbore Shape

Figures 72 and 73 show the hoop stress distribution for imperfect wellbore shapes exposed to 7000 psi and 10000 psi wellbore pressures. When the wellbore shape is not perfect and the wellbore pressure is 7000 psi, there is only one crack at the wellbore wall. By increasing wellbore pressure, the other crack is generated. As a result, when the wellbore shape is not perfectly circular, the cracks are not opened at the same time and they are not symmetric. The first crack is opened and by increasing wellbore pressure, the second one is opened at the wall. The hoop stresses before the cracks are initiated; after initiated; and after propagated are shown in Figure 72 and 73.Also, in Figure 74 and 75 the hoop stress distributions and multiple cracks are shown.

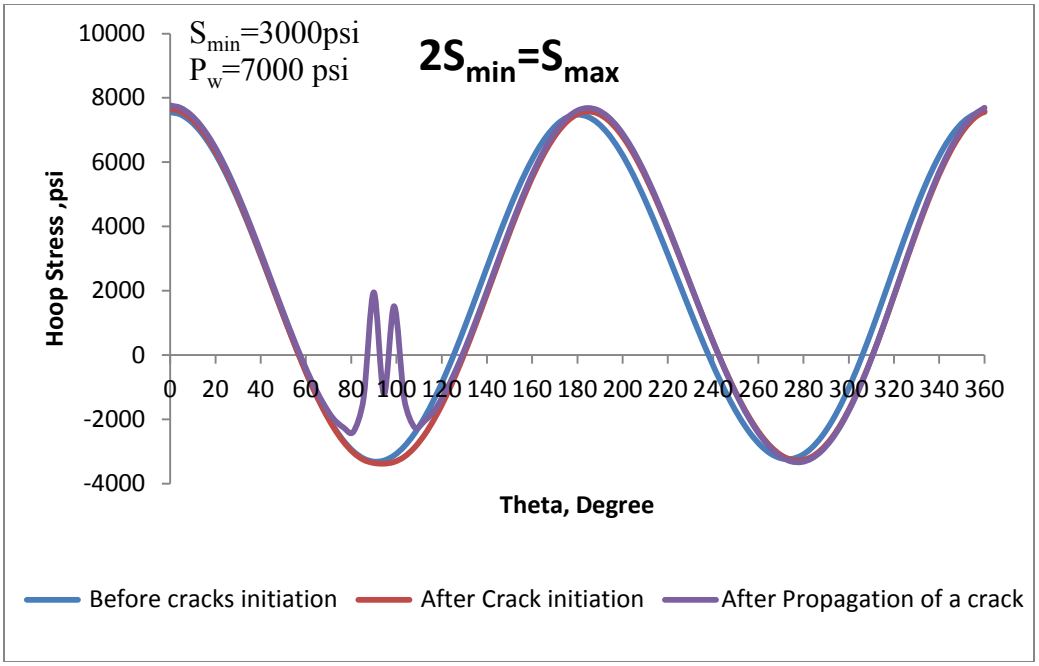

Figure 72. Hoop stress distribution for multiple cracks in imperfect wellbore shape, P_w=7000 psi

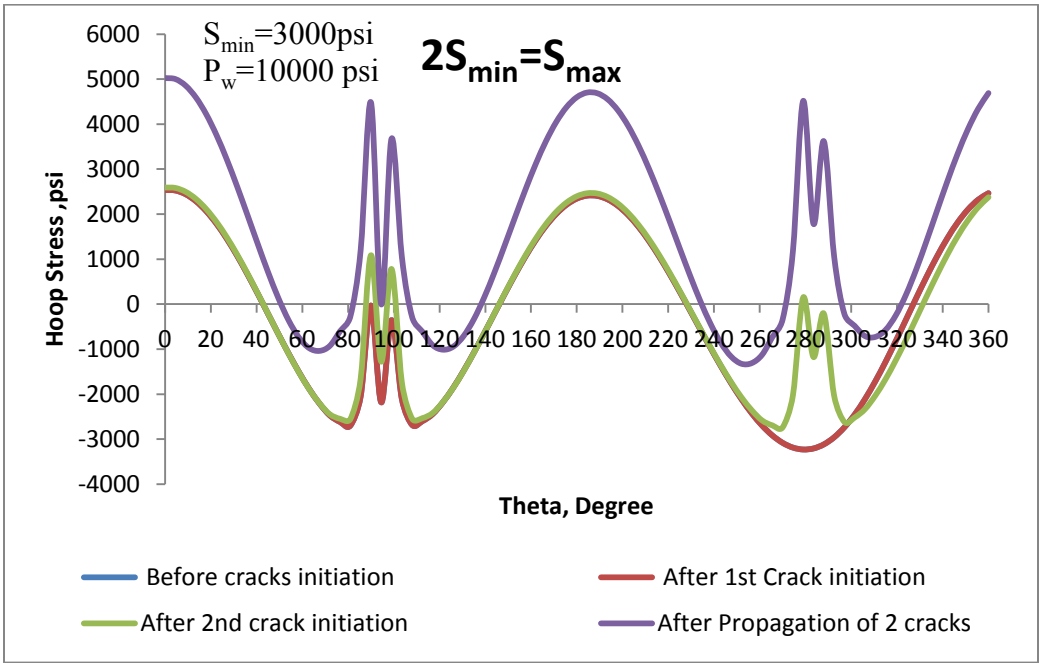

Figure 73. Hoop stress distribution for multiple cracks in imperfect wellbore shape, P_w=10000 psi

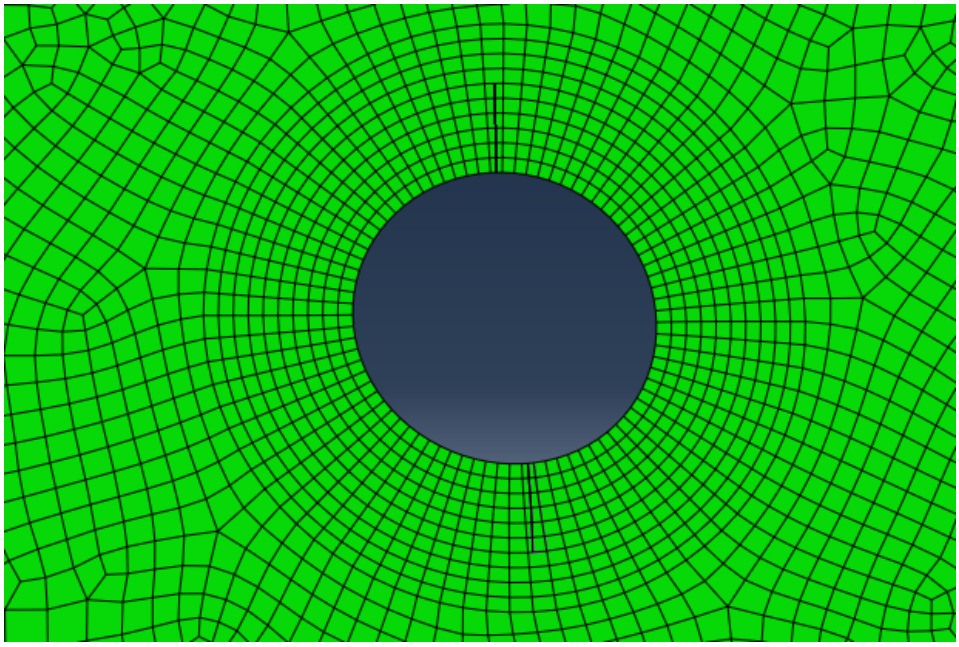

Figure 74. Multiple cracks in imperfect wellbore shape, P_w=10000 psi, ABAQUS

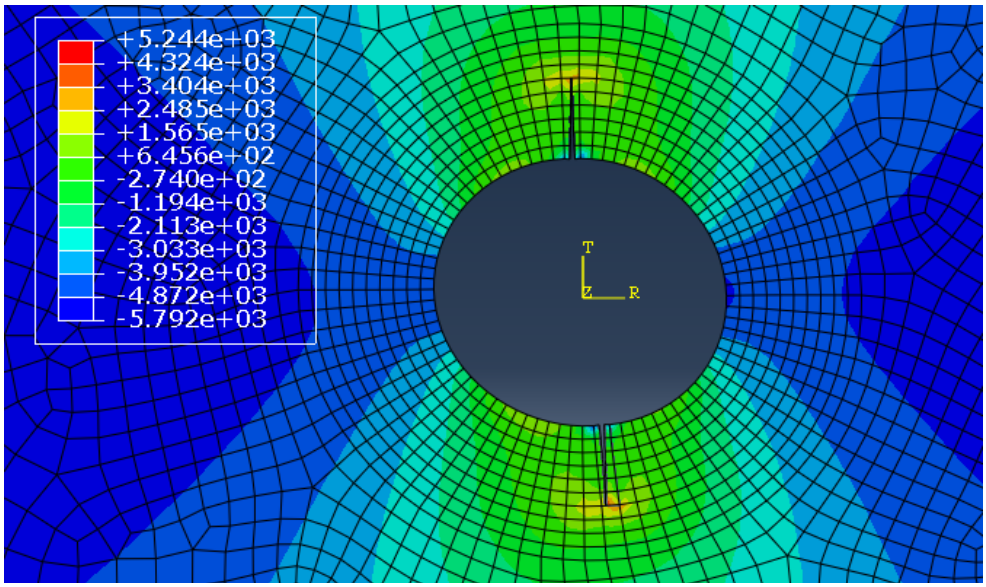

Figure 75. Hoop stress distribution for multiple cracks in imperfect wellbore shape, P_w=10000 psi, ABAQUS

4.4.4. Comparison of Hoop Stress Distribution between Perfect and Imperfect Wellbore Shape

When the perfection of wellbore shape is compared, it be concluded that, the cracks are not symmetric in an imperfect wellbore. However, the cracks positions are symmetric at the wellbore wall in a perfectly circular wellbore. Furthermore, the cracks are opened at the same time in a perfect circular wellbore and propagate together. On the other hand, when the wellbore shape is not perfect, cracks are not open at the same time and one crack is opened and propagated right after the other one. Figures 76 and 77 show the hoop stress comparison between perfect and imperfect wellbore shapes. These are graphs of crack propagation hoop stresses. For instance, from Figure 76, when wellbore pressure is 7000 psi, there is only one crack if the wellbore shape is imperfect. On the other hand, when all the situations are the same, there are two cracks when the wellbore shape is perfectly circular. Finally, all the features of cracks are changed by changing perfection of wellbore shape.

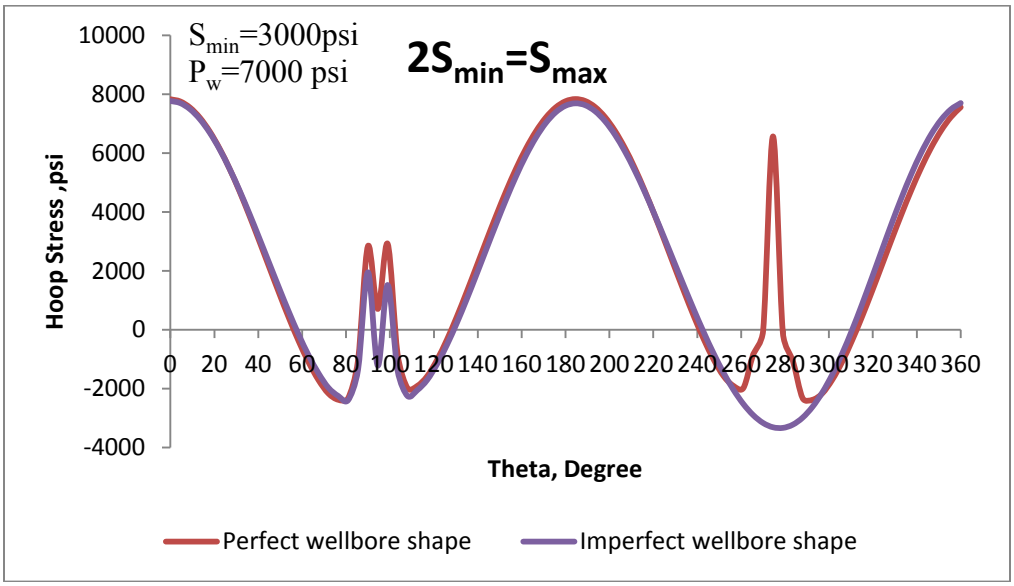

Figure 76. Comparison of hoop stress distribution for multiple cracks in imperfect wellbore shape, P_w=7000 psi

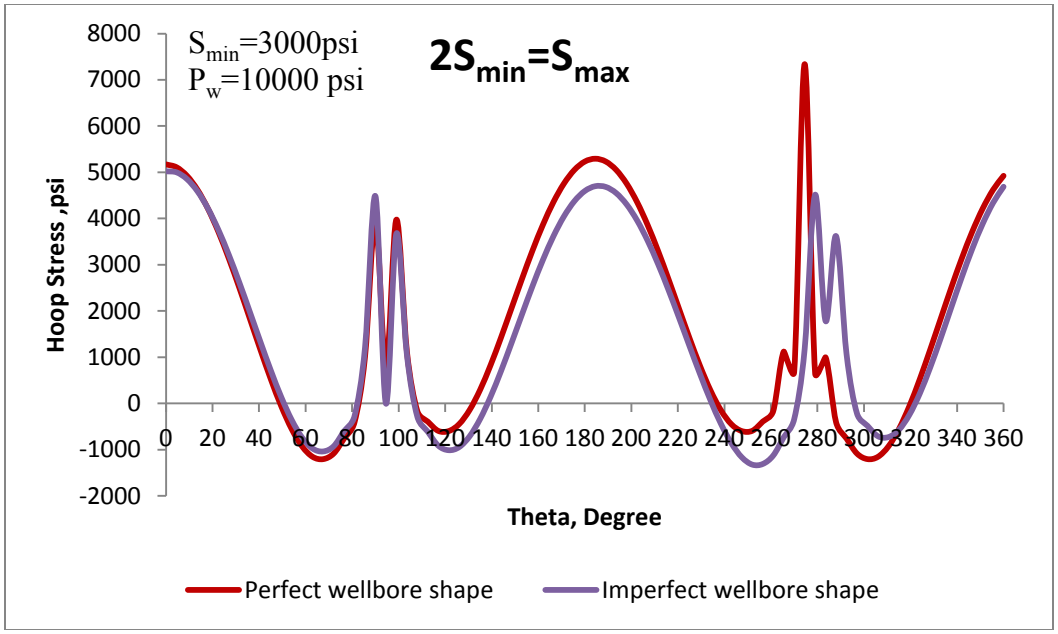

Figure 77. Comparison of hoop stress distribution for multiple cracks in imperfect wellbore shape, P_w=10000 psi

5. Summary, Conclusions and Future Work

In this study, casing drilling and the smearing effect of casing drilling are examined to better understand the smear effect and its potential in "undrillable formations". It is concluded that smearing effect of casing drilling is one of the most important advantages to prevent lost circulation and strengthen the wellbore effectively.

Computational models were created to analyze hoop stresses around the wellbore wall using ABAQUS. With such models smearing effect results can be used as a tool to estimate real stress fields around the wellbore. Also, the effect of Young's modulus; pore pressure; pore fluid flow velocity; bridging location; multiple cracks effects; and wellbore shape are examined.

The hoop stress analysis of models without pore pressure, with pore pressure and pore fluid flow are presented and show that when the horizontal stress anisotropy is high, the smearing effect is more effective than low stress anisotropy.

It is also concluded that the smearing particles should be close to the fracture mouth to plug the fracture and achieved perfect sealing. Different scenarios were examined as 0.5 in., 1 in., 2 in., 3 in., bridge location inside 6 inch fractures and it was shown that the closer the sealing location, the better the smearing.

When the model contains pore fluid, the fracture closure is higher than without pore pressure. Pore fluid has a positive effect for fracture closure, but it decreases hoop stresses around the wellbore. When pore fluid flow velocity is high, pore pressure distribution increases and changes the hoop stress distribution around the wellbore wall. It is concluded that the effects of including pore pressure in the simulation are more important than without pore pressure models.

Multiple fracture effects were investigated on hoop stress distribution around the wellbore and also the wellbore shape. When there are multiple cracks, the hoop stress increase is achieved between the cracks which are the result of compression of the adjacent formation by opening cracks. Also, when the wellbore shape is perfect circular, the fractures open at the same time and propagate together by changing pressure. On the other hand, when the wellbore shape is imperfect as not a circle, the fractures open at different times. One opens first and starts to propagate, the other one opens and propagates. In addition, as a result of perfection, the cracks are symmetric at the wellbore wall. On the other hand, if cracks are not symmetric when the wellbore shape is not perfectly circular and thus, they do not open and propagate together. It is concluded that imperfection as not a circle at the wellbore wall affects the hoop stresses and the location of the cracks.

Future Work:

To improve future work, models can be examined in three dimensions and intensive lab experiments are recommended to verify results in this study. Also, mud properties can be added to illustrate differences between the models with and without mud. Mud invasion into the fracture, which creates internal and external mud cake situations, should be investigated. Moreover, the particle sizes of the smearing formations can be investigated to see the sealing efficiency of different particle size distributions. Finally, field experiments are recommended to verify these results under real conditions.

References

ABAQUS/CAE 6.10 EF, Analysis User's Manual, 2010.

Adams, H.A., Rosenberg, S., Montgomery, M., Galloway, G., "Drilling with Casing Overcomes Losses to Thief Zone", OTC 17687, Offshore Technology Conference, Houston, Texas, May 2-5, 2005.

Alberty, M.W. and Mclean, M. R. "A Physical Model for Stress Cages", SPE 90493, SPE Annual Technical Conference, Houston, September 26-29, 2004.

Amaco Wellbore Stability Drilling Handbook.

Aston, M. S., Alberty, M.W., Mclean, M. R., de Jong, H.J. and Armagost, K. "Drilling Fluids for Wellbore Strengthening", SPE 87130, SPE/IADC Drilling Conference, Dallas, March 2-4,2004.

Aston, M.S. et al. "A New Treatment for Wellbore Strengthening in Shale", SPE 110713, SPE Annual Technical Conference and Exhibition, Anaheim California, USA, November 11-14, 2007.

Chilingarian G., Voraburt, P. "Drilling and Drilling Fluids", 1st edition, Elsevier Scientific Publishing Company, New York, USA, 1983.

Dupriest, F.E. "Fracture Closure Stress (FCS) and Lost Returns Practices" SPE 92192, SPE/IADC Drilling Conference, Amsterdam, February 23-25, 2005.

Fisher, A., Reid, D., Tan, M.Z., Galloway, G., "Extending the Boundaries of Casing Drilling", SPE 87998, IADC/SPE Asia Pacific Drilling Technology Conference and Exhibition, Kuala Lumpur, Malaysia, September 13-15, 2004.

Fontenot, Kyle, Highnote, Joe, Warren, Tommy and Houtchens, Bruce "Casing Drilling Activity Expands in South Texas" SPE 79862, SPE/IADC Drilling Conference, Amsterdam, February 19-21,2003.

Fontenot, Kyle, Warren, Tommy and Houtchens, Bruce "Casing Drilling proves successful in South Texas" World Oil, October 2002, pp 27-32.

Fontenot, K, et al, "Improved Wellbore Stability Achieved with Casing Drilling Operations through Drilling Fluids "Smear Effect", World Oil 2004 Casing Drilling: Technical Conference, Houston, TX, March 30-31, 2004

Fuh, G-F., Morita, N. Boyd, P.A. and McGoffin, S.J. "A New Approach to Preventing Lost Circulation while Drilling," SPE 24599, 67th Annual Technical Conference and Exhibition, Washington D.C., October 4-7, 1992.

Gallardo H., Cassanelli J.P., Barret S., Romero P., Mufarech A., "Casing-Drilling Technology (CwD) Mitigates Fluid Losses in Peruvian Jungle" SPE 139065 SPE Latin American & Caribbean Petroleum Engineering Conference, Lima, Peru, December 1-3, 2010.

Gupta, A.K., “Drilling with Casing: Prospects and Limitations”, SPE 99536, SPE Western Regional/AAPG Pacific Section/ GSA Cordilleran Section Joint Meeting, Anchorage, Alaska, USA, May 8-10, 2006.

Hossain, M.M., Amro, M.M., “Prospects of Casing While Drilling and the Factors to be Considered during Drilling Operations in Arabian Region”, IADC/SPE 87987, IADC/SPE Asia Pacific Drilling Technology Conference, Kuala Lumpur, Malaysia, September 13-15, 2004.

Houtcehens, B., Foster, J., Tessari, R., “Applying Risk Analysis to Casing While Drilling”, SPE/IADC 105678, SPE/IADC Drilling Conference, Amsterdam, Netherlands, February 20-22, 2007.

Hubbert, M. K. and Willis, D. G., “Mechanics of Hydraulic Fracturing”, Trans. AIME, Vol 210, pp-153-166, 1957.

Ivan, C., Bruton, J., “How Can We Best Manage Lost Circulation”, AADE-03-NTCE-38, AADE National Technology Conference, Houston, Texas, April 1-3, 2003.

Kardos, M., “Drilling with Casing Gains Industry Acceptance”, American Oil & Gas Reporter, April 2008.

Karimi, M., Ghalambor, A., Montgomery, M., Moellendick, E., “Formation Damage and Fluid Loss Reduction due to Plastering Effect of Casing Drilling”, SPE 143656, SPE European Formation Damage Conference, Noordwijk, Netherlands, June 7-10, 2011.

Limbert, D., et al. “Evolution of Drillable PDC Technology Enables Operators to Safely and Economically Drill South Texas Gas Wells with Casing”, SPE/IADC 119422, SPE/IADC Drilling Conference and Exhibition, Amsterdam, Netherlands, March 17-19, 2009.

Lopez E., Bonilla P., Castilla A., Rincon J., “Casing Drilling Application with Rotary Steerable and Triple Combo in New Deviated Wells in Cira Infantas Field”, SPE 134586, SPE Annual Technical Conference and Exhibition, Florence, Italy, September 19-20, 2010.

Lopez, E.A., Bonilla, P.A., “Casing Drilling Application in the Depleted La Cira Infantas Mature Field Colombia”, SPE 139020, SPE Latin American & Caribbean Petroleum Engineering Conference, Peru, December 1-3, 2010.

Messenger, J. U.: *Lost Circulation*, PennWell Publishing Company, Tulsa, Oklahoma, 1981.

Moellendick. E.: “Casing Drilling Improves Mature Field Production, Eliminates Fluid Losses, Directionally Drills Wells” Drilling Contractor, page 76-79, July/August 2008.

Moellendick, E., Karimi, M., “How Casing Drilling Improves Wellbore Stability”, AADE-11-NTCE-64, AADE National Technical Conference, Houston, Texas, April 12-14, 2011.

Morita, N., Black, A. D., and Fuh, G. F., "Theory of Lost Circulation Pressure," SPE 20409, 65th Annual Technical Conference and Exhibition of the Society of Petroleum Engineers, pp. 43-58, 1990.

Rahman, H., “Detection, Mechanism and Control of Lost Circulation in Drilling”, Master’s Thesis, Dalhousie University, April 2010.

Robinson, Shon D., Bealessio, Tom M., Shafer, Randall S., ConocoPhillips Company, “Casing Drilling in the San Juan Basin to Eliminate Lost Returns in a Depleted Coal Formations”, IADC/SPE 112545, IADC/SPE Drilling Conference, Orlando, Florida, USA, March 4-6, 2008.

Salehi, S., Nygaard, R., “Evaluation of New Drilling Approach for Widening Operational Window: Implications for Wellbore Strengthening”, SPE 140753, SPE Production and Operations Symposium, Oklahoma City, Oklahoma, USA, March 27-29, 2011.

Shepard, S. F., Reiley, R. H., and Warren, T. M., “Casing Drilling: An Emerging Technology”, IADC/SPE 67731, IADC/SPE Drilling Conference, Amsterdam, February 27-March 1, 2001.

Shepard, S.F. ,Reiley, R.H. and Warren, T. :”Casing Drilling Successfully Applied in Southern Wyoming”, World Oil, p. 33-41, June 2002.

SPE Distinguished Lecturer Series, SPE 112819.

Tessari. R. M., Madell, Garret, Warren, Tommy, “Drilling with Casing Promises Major Benefits”, Oil and Gas Journal, Vol. 97 No. 20, May 17, 1999, pp 58-62.

Tessari M., Warren T., Jo J. Y., “Drilling with Casing Reduces Cost and Risk” SPE 101819, SPE Russian Oil and Gas Technical Conference and Exhibition, Moscow, Russia, October 3-6, 2006.

Van Oort, E. Friedheim, J., Pierce, T., Lee, J., “Avoiding Losses in Depleted and Weak Zones by Constantly Strengthening Wellbores”, SPE 125093, SPE Annual Technical Conference and Exhibition, New Orleans, Louisiana, USA, October 4-7, 2009.

Wang, H. et al. “Fractured Wellbore Stress Analysis- Can Sealing Micro-Cracks Really Strengthen a Wellbore?”, SPE/IADC 104947, SPE/AIDC Drilling Conference, Amsterdam, February 20-22, 2007.

Wang, H, Tower, B.F. and Mohamed, S.Y. “Near Wellbore Stress Analysis and Wellbore Strengthening for Drilling Depleted Formations”, SPE 102719, SPE Rocky Mountain Oil & Gas Technology Symposium, Denver, Colorado, USA, April 16-18, 2007.

Wang, H., et al. “Investigation of Factors for Strengthening a Wellbore by Propping Fractures”, SPE/IADC 112629, IADC/SPE Drilling Conference, Orlando, Florida, March 4-6, 2008.

Warren, T., Houtchens, B., Madell, G., “Directional Drilling with Casing”, SPE/IADC 79914, SPE/IADC Drilling Conference, Amsterdam, February 10-21, 2003.

Warren, T., Lesso, B., “Casing Drilling Directional Wells”, OTC 17453, Offshore Technology Conference, Houston, TX, USA, May 2-5, 2005.

Warren, T. and Tessari, R., “Casing Drilling with Retrievable Drilling Assemblies” OTC 16564, Offshore Technology Conference, Houston, USA, May 3-6, 2006

Watts. R.D., Greener. M.R., McKeever. S., Scott. P.D.,Beardmore. D., : “Particle Size Distribution Improves Casing-While-Drilling Wellbore Strengthening Results” IADC/SPE 128913, IADC/SPE Drilling Conference & Exhibition, New Orleans, Louisiana, February 2-4, 2010.

Zeilinger, S. “Lost Returns and Stress Building”, Drilling Technical/Operations Support, November 2010.